The Center for Night Vision and Electro-Optics

OPTOELECTRONIC WORKSHOPS

VIII

QUANTUM-LIMITED IMAGING AND IMAGE PROCESSING

July 12, 1988

sponsored jointly by

ARO-URI Center for Opto-Electronic Systems Research
The Institute of Optics, University of Rochester

UNCLASSIFIED
SECURITY CLASSIFICATION OF THIS PAGE

REPORT DOCUMENTATION PAGE

1a. REPORT SECURITY CLASSIFICATION Unclassified	1b. RESTRICTIVE MARKINGS
2a. SECURITY CLASSIFICATION AUTHORITY	3. DISTRIBUTION / AVAILABILITY OF REPORT Approved for public release; distribution unlimited.
2b. DECLASSIFICATION / DOWNGRADING SCHEDULE	
4. PERFORMING ORGANIZATION REPORT NUMBER(S)	5. MONITORING ORGANIZATION REPORT NUMBER(S) ARO 24626.77-PH-UIR
6a. NAME OF PERFORMING ORGANIZATION University of Rochester 6b. OFFICE SYMBOL (If applicable)	7a. NAME OF MONITORING ORGANIZATION U. S. Army Research Office
6c. ADDRESS (City, State, and ZIP Code) The Institute of Optics Rochester, NY 14627	7b. ADDRESS (City, State, and ZIP Code) P. O. Box 12211 Research Triangle Park, NC 27709-2211
8a. NAME OF FUNDING / SPONSORING ORGANIZATION U. S. Army Research Office 8b. OFFICE SYMBOL (If applicable)	9. PROCUREMENT INSTRUMENT IDENTIFICATION NUMBER DAAL03-86-K-0173
8c. ADDRESS (City, State, and ZIP Code) P. O. Box 12211 Research Triangle Park, NC 27709-2211	10. SOURCE OF FUNDING NUMBERS PROGRAM ELEMENT NO. / PROJECT NO. / TASK NO. / WORK UNIT ACCESSION NO

11. TITLE (Include Security Classification)
Optoelectronic Workshop VIII: Quantum-Limited Imaging and Image Processing

12. PERSONAL AUTHOR(S)
G. Michael Morris

13a. TYPE OF REPORT	13b. TIME COVERED	14. DATE OF REPORT (Year, Month, Day)	15. PAGE COUNT
Technical	FROM _____ TO _____	July 12, 1988	

16. SUPPLEMENTARY NOTATION
The view, opinions and/or findings contained in this report are those of the author(s) and should not be construed as an official Department of the Army position, policy, or decision, unless so designated by other documentation.

17. COSATI CODES		
FIELD	GROUP	SUB-GROUP

18. SUBJECT TERMS (Continue on reverse if necessary and identify by block number)
Workshop; quantum-limited imaging; image processing

19. ABSTRACT (Continue on reverse if necessary and identify by block number)

This workshop on "Quantum-Limited Imaging and Image Processing" represents the eighth of a series of intensive academic/ government interactions in the field of advanced electro-optics, as part of the Army sponsored University Research Initiative. By documenting the associated technology status and dialogue it is hoped that this baseline will serve all interested parties towards providing a solution to high priority Army requirements. Responsible for program and program execution are Dr. Nicholas George, University of Rochester (ARO-URI) and Dr. Rudy Buser, NVEOC.

20. DISTRIBUTION / AVAILABILITY OF ABSTRACT	21. ABSTRACT SECURITY CLASSIFICATION	
☐ UNCLASSIFIED/UNLIMITED ☐ SAME AS RPT. ☐ DTIC USERS	Unclassified	
22a. NAME OF RESPONSIBLE INDIVIDUAL Nicholas George	22b. TELEPHONE (Include Area Code) 716-275-2417	22c. OFFICE SYMBOL

DD FORM 1473, 84 MAR — 83 APR edition may be used until exhausted. All other editions are obsolete.

SECURITY CLASSIFICATION OF THIS PAGE
UNCLASSIFIED

OPTOELECTRONIC WORKSHOP

ON

QUANTUM-LIMITED IMAGING AND IMAGE PROCESSING

Organizer: ARO-URI-University of Rochester
and Center for Night Vision and Electro-Optics

1. INTRODUCTION

This workshop on "Quantum-Limited Imaging and Image Processing" represents the eighth of a series of intensive academic/ government interactions in the field of advanced electro-optics, as part of the Army sponsored University Research Initiative. By documenting the associated technology status and dialogue it is hoped that this baseline will serve all interested parties towards providing a solution to high priority Army requirements. Responsible for program and program execution are Dr. Nicholas George, University of Rochester (ARO-URI) and Dr. Rudy Buser, NVEOC.

2. SUMMARY AND FOLLOW-UP ACTIONS

Opening remarks were by Dr. Rudy Buser. In his introduction he summarized the scientific and technology missions of NVEOC He indicated a strong interest in exploring approaches to automatic target recognition (ATR), particularly those which may be useful for automatic recognition of military targets located in a cluttered environment.

Dr. Michael Morris followed withan overview of the work being done at the Institude of Optics on quantum-limited imaging and image processing. He discussed an approach to ATR in which a quatum-limited image, i.e. consisting of only a few detected photoevents, is correlated with a reference function located in computer memory. A key feature of the method is that it provides a simple way to reduce the amount of information that must be processed to make reliable recognition decisions.

Next, three graduate students, working with Dr. Morris at the University of Rochester, described the main results obtained from their dissertation research. Thomas Isberg discussed his work on rotation-invariant filtering using circular-harmonic expansions, and two-staged template matching. Miles Wernich presented work on maximum-likihood image classification, stressing the importance of filter designs, which are insentive to intrinsic object variations with a given class. Edward Watson described methods to upconvert (both narrow and Broadband) infrared images to a visible-wavelength range, in which focal-plane detector arrays are readily available.

Dr. David Singer presented an overview of the work at NVEOC on image processing and ATR, with emphasis on model-based, multi-sensor algorithm development.

The final presentation was given by Teresa Kipp, NVEOC, on laser radar imaging. Effects of sampling, field of view, noise, ambiguity interval on laser imagery were illustrated. Examples of the use of range data to for 3-d surface profile images were also discussed.

From the workshop the following areas for continued interaction have been identified:

a. Specialize the University of Rochester's ATR scheme for the recognition of laser radar imagery, and compare its performance with NVEOC algorithums. NVEOC will provide the University of Rochester with laser radar imagery.

b. Initiate interaction with NVEOC personnel on methods for generating upconverted imagery, and identify specific military applications.

c. Model the manner in which speckle noise distorts a modulated laser radar beam. In turn, on the basis of this work. NVEOC will model the probability distribution of error in range measurements.

CENTER FOR OPTO-ELECTRONIC SYSTEMS RESEARCH
BASIC PRINCIPLES AND OVERVIEW

N=20M

N=64K

N=16K

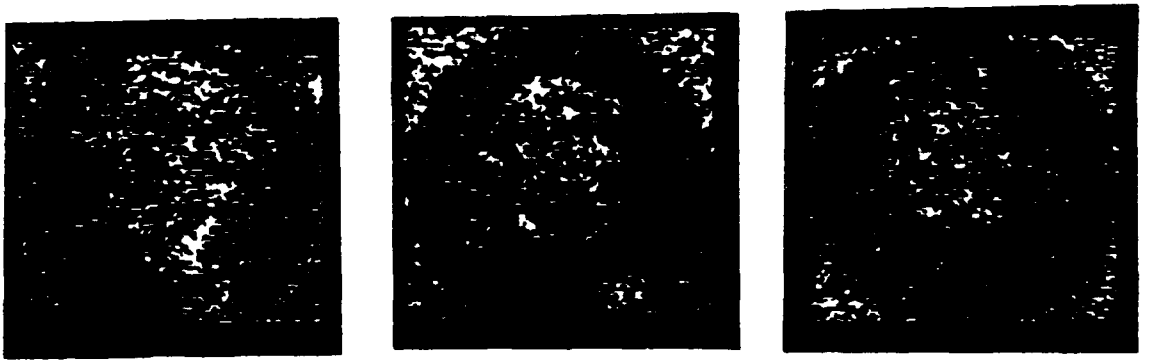

N=4K

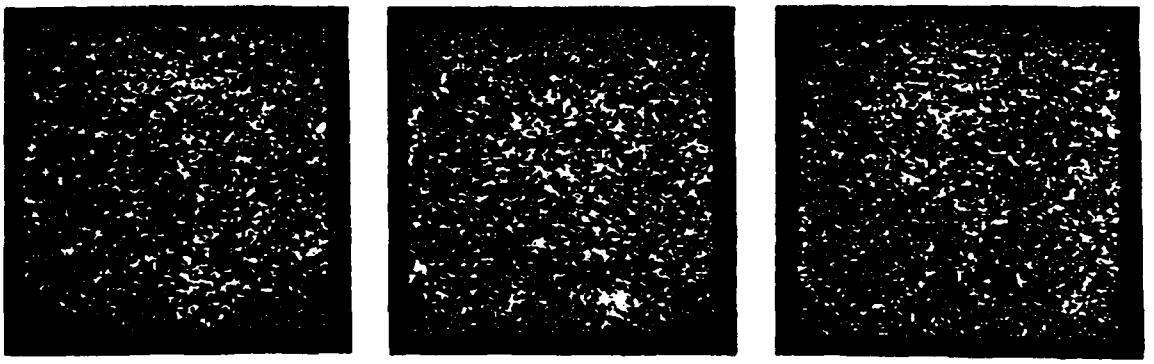

N=1K

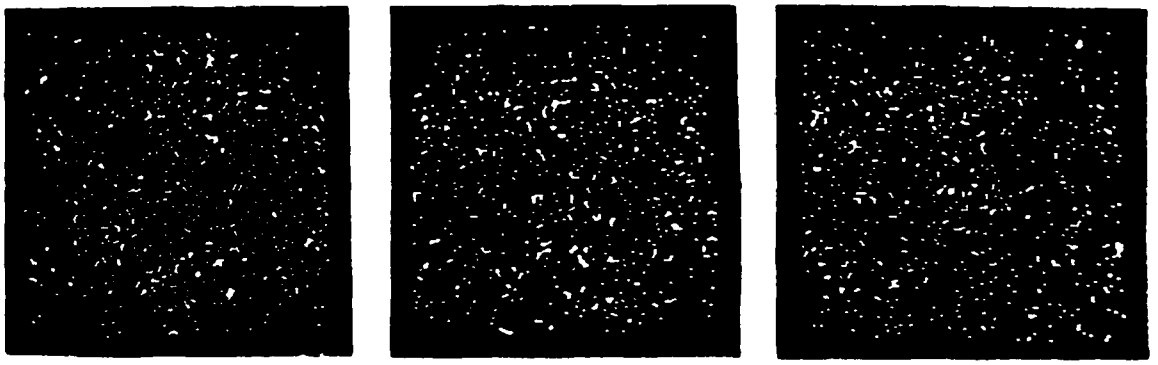

ROC Curves
Washington and Lincoln

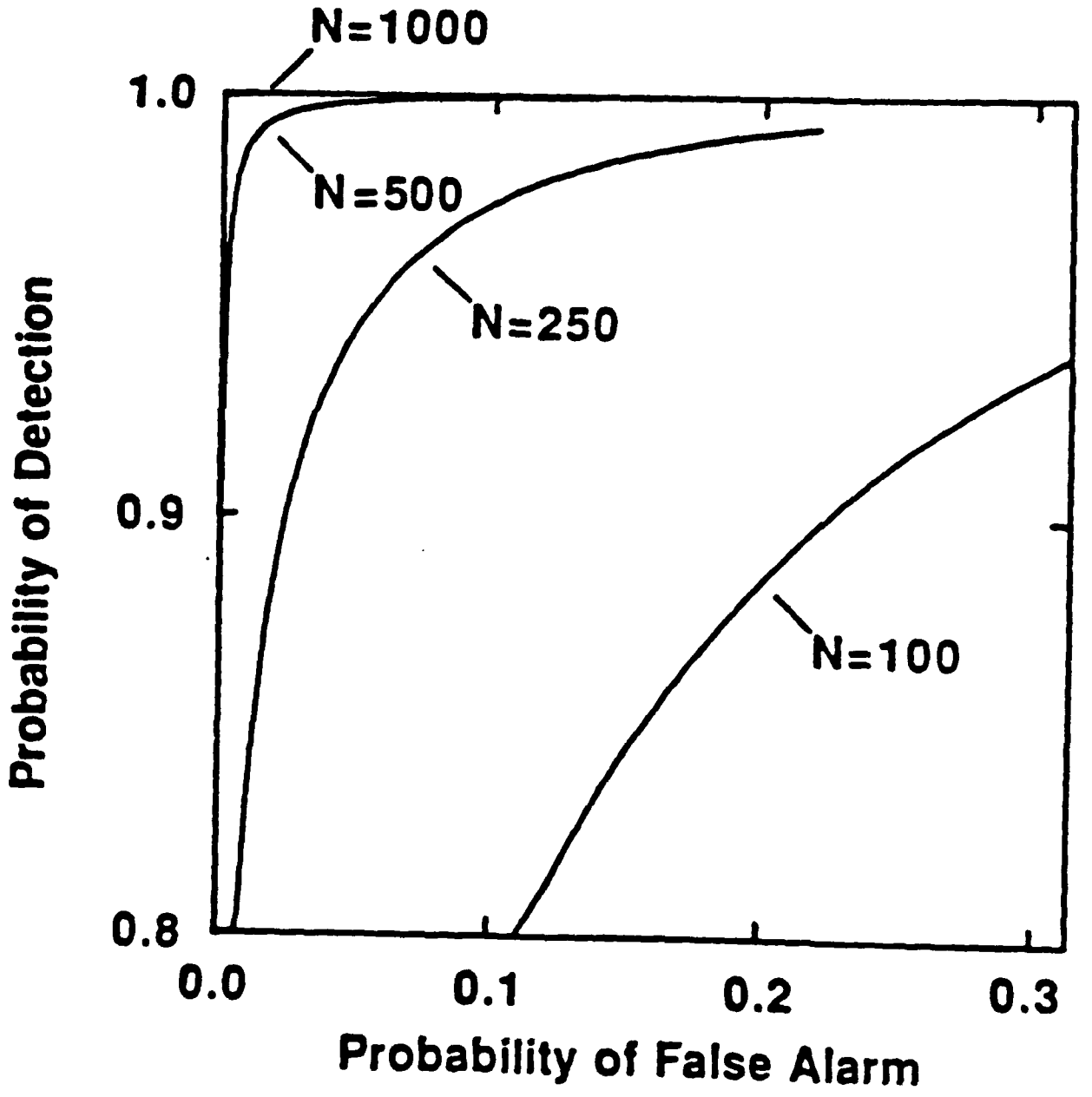

Resistive-Anode, Photon-Counting Detection System

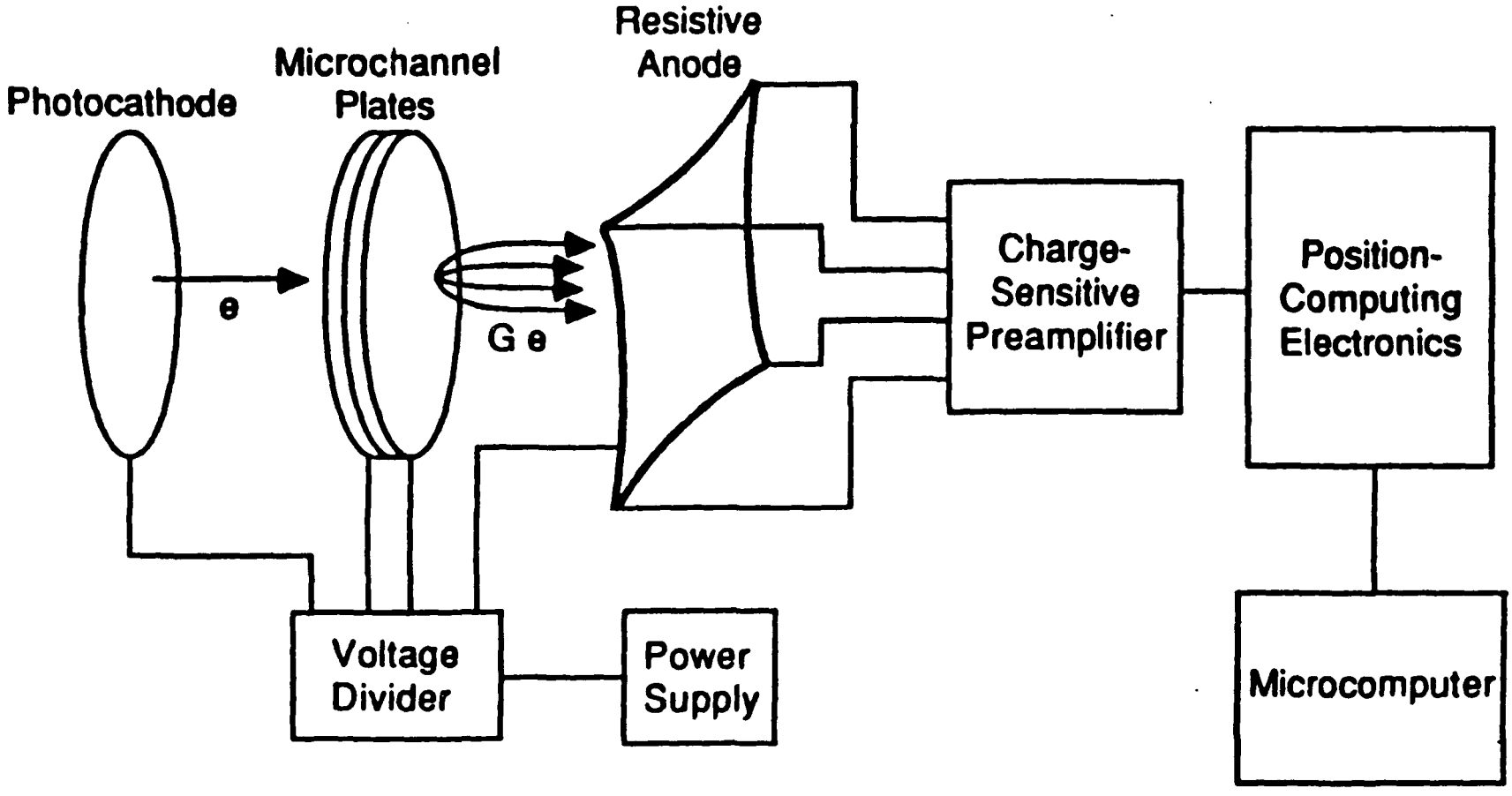

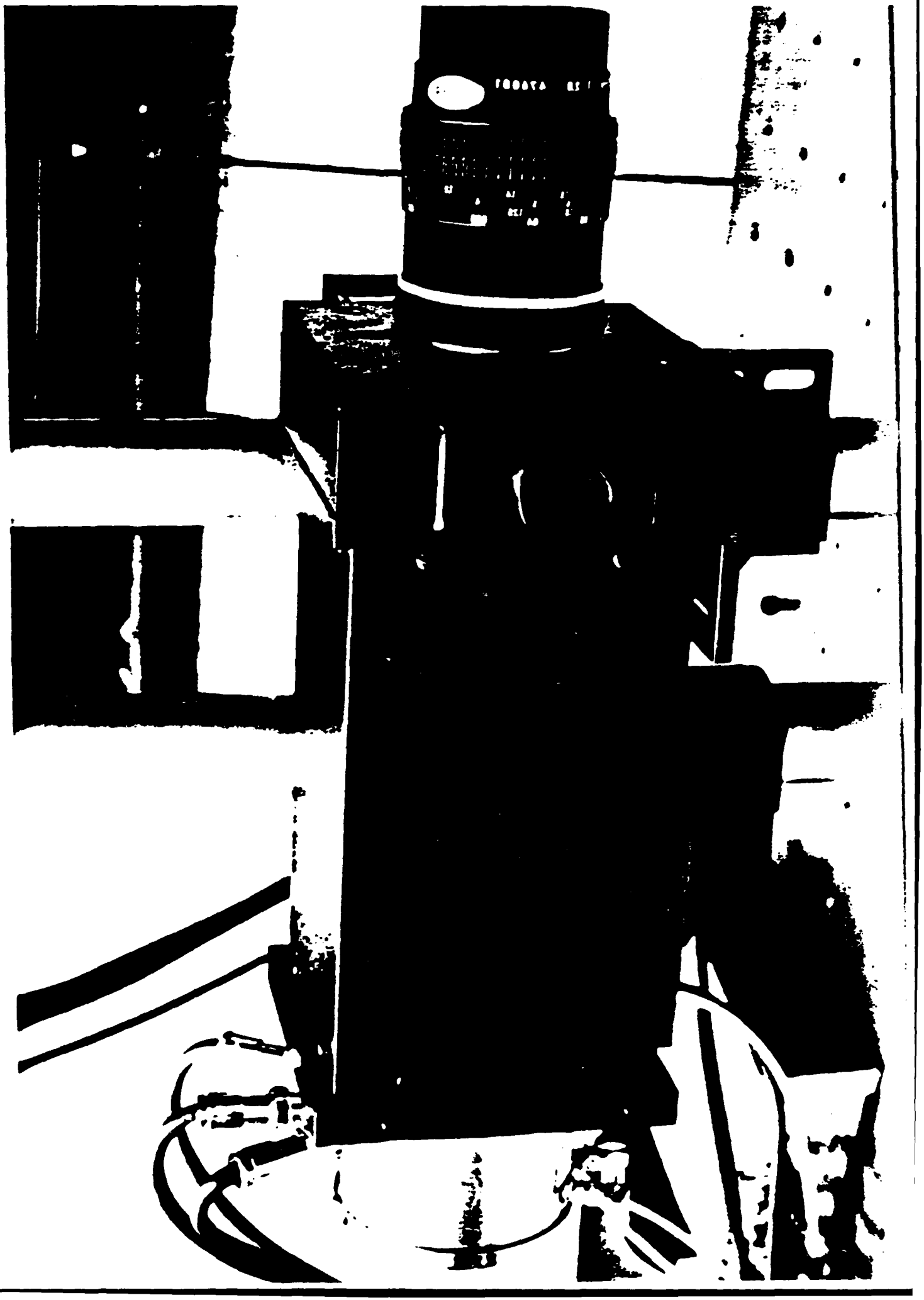

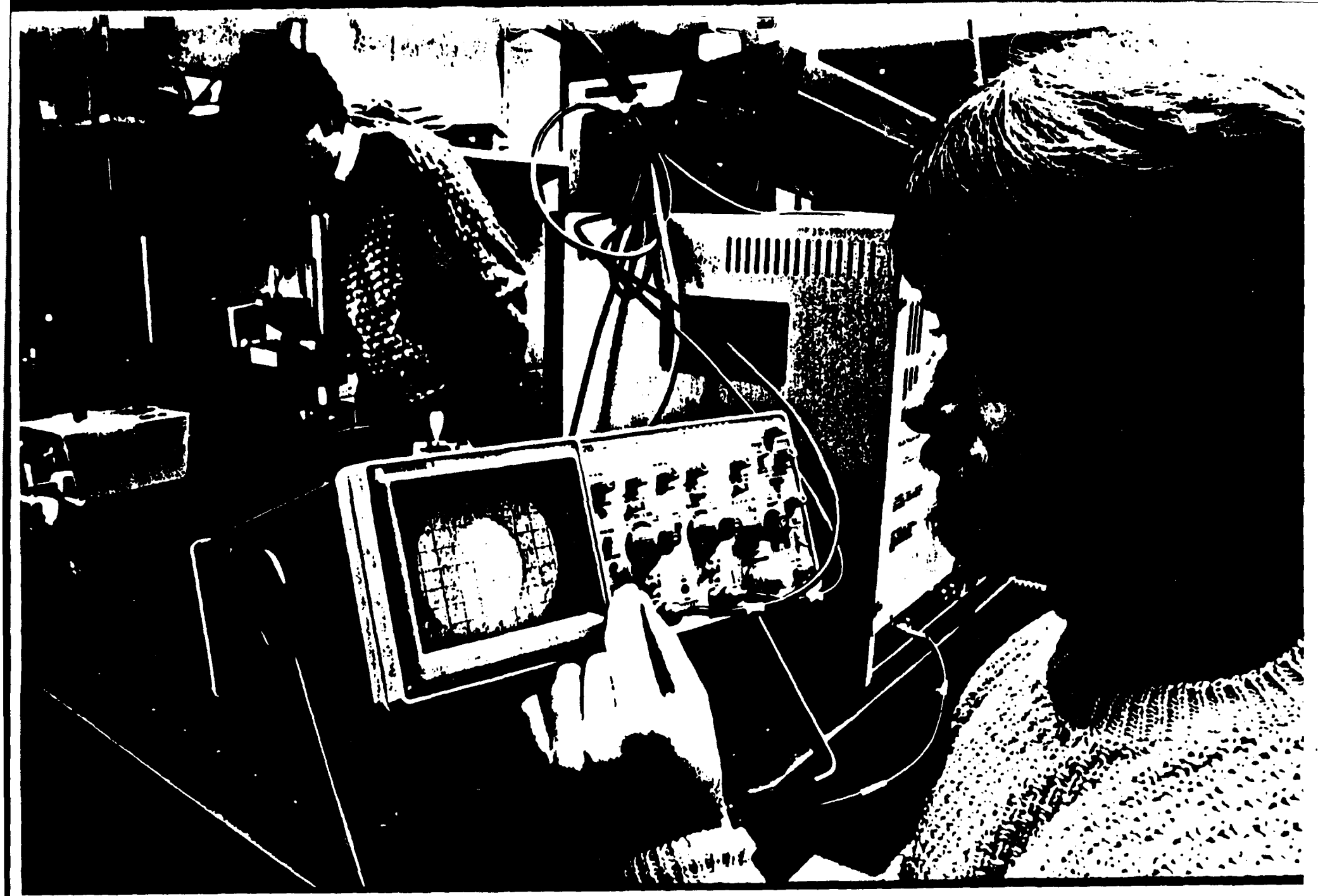

IMAGE RECOGNITION AT LOW LIGHT LEVELS

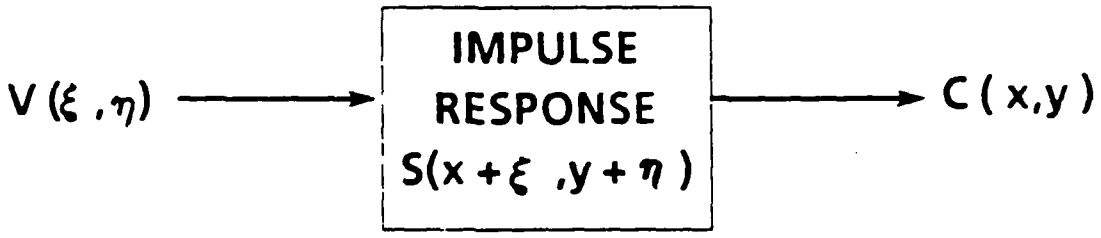

$$\text{INPUT SCENE: } V(\xi,\eta) = \sum_{i=1}^{M} \delta(\xi - x_i, \eta - y_i)$$

STORED REFERENCE FUNCTION: $S(\xi,\eta)$

CORRELATION SIGNAL:

$$C(x,y) = \iint_{A} d\xi\, d\eta\, V(\xi,\eta)\, S(x+\xi, y+\eta)$$

$$C(x,y) = \sum_{i=1}^{N} S(x-x_i, y-y_i)$$

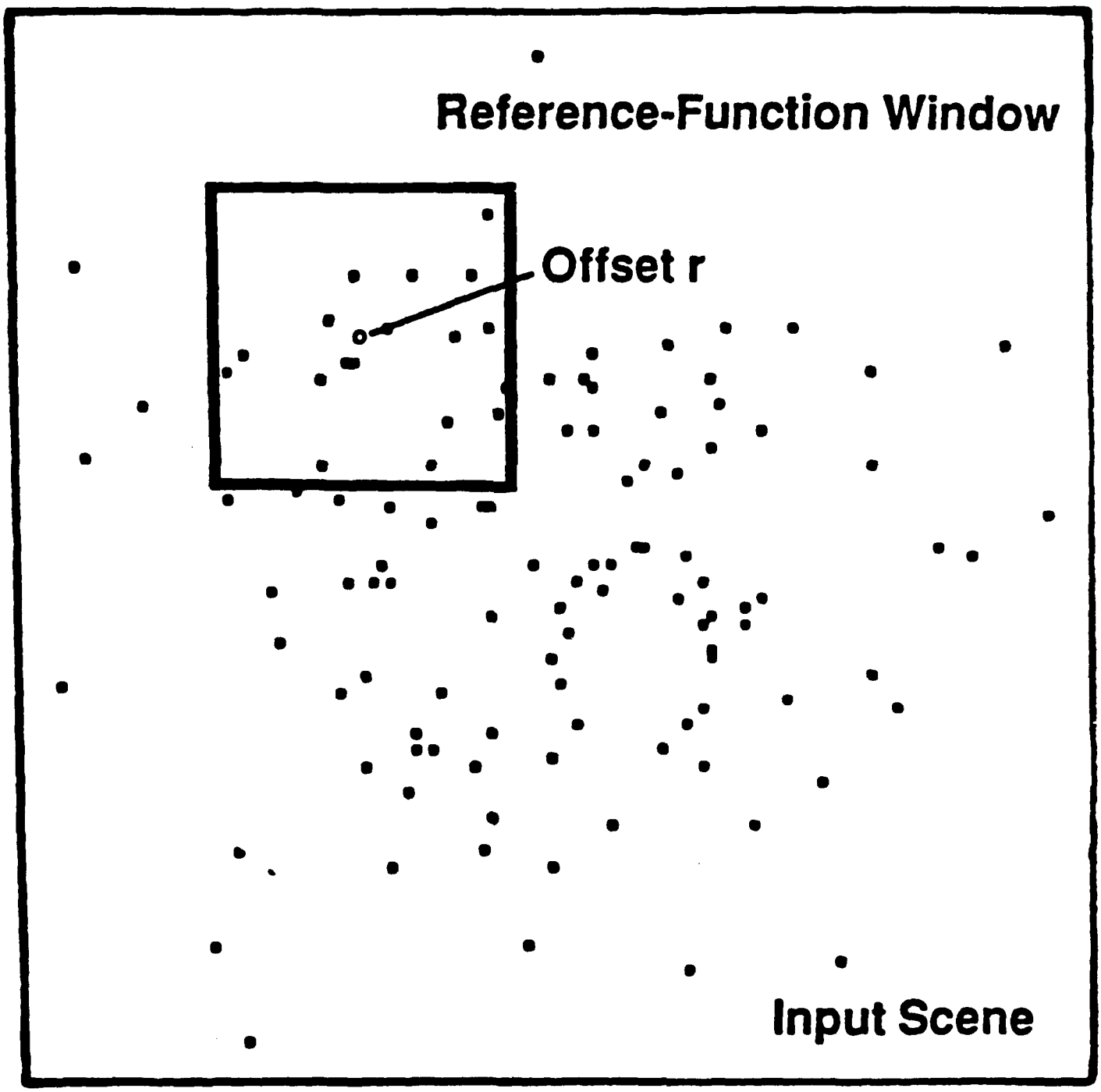
Reference-Function Window
Offset r
Input Scene

$$C(x,y) = \sum_{i=1}^{N} S(x+x_i, y+y_i)$$

CORRELATION STATISTICS
LARGE $\overline{N}$

GAUSSIAN PDF

$$P\left[C(x,y)\right] = \frac{1}{\sigma\sqrt{2\pi}} e^{-\frac{\left[C(x,y) - \langle C(x,y)\rangle\right]^2}{2\sigma^2}}$$

EXPECTED VALUE

$$\langle C(x,y)\rangle = \frac{\eta\tau}{h\nu_o} \iint_A d\xi\, d\eta\, V(\xi,\eta) S(x+\xi, y+\eta)$$

VARIANCE

$$\sigma^2_{C(x,y)} = \frac{\eta\tau}{h\nu_o} \iint_A d\xi\, d\eta\, V(\xi,\eta) S^2(x+\xi, y+\eta)$$

Detection Criterion

H_0: Reference object <u>is not</u> present in the input scene

H_1: Reference object <u>is</u> present in the input scene

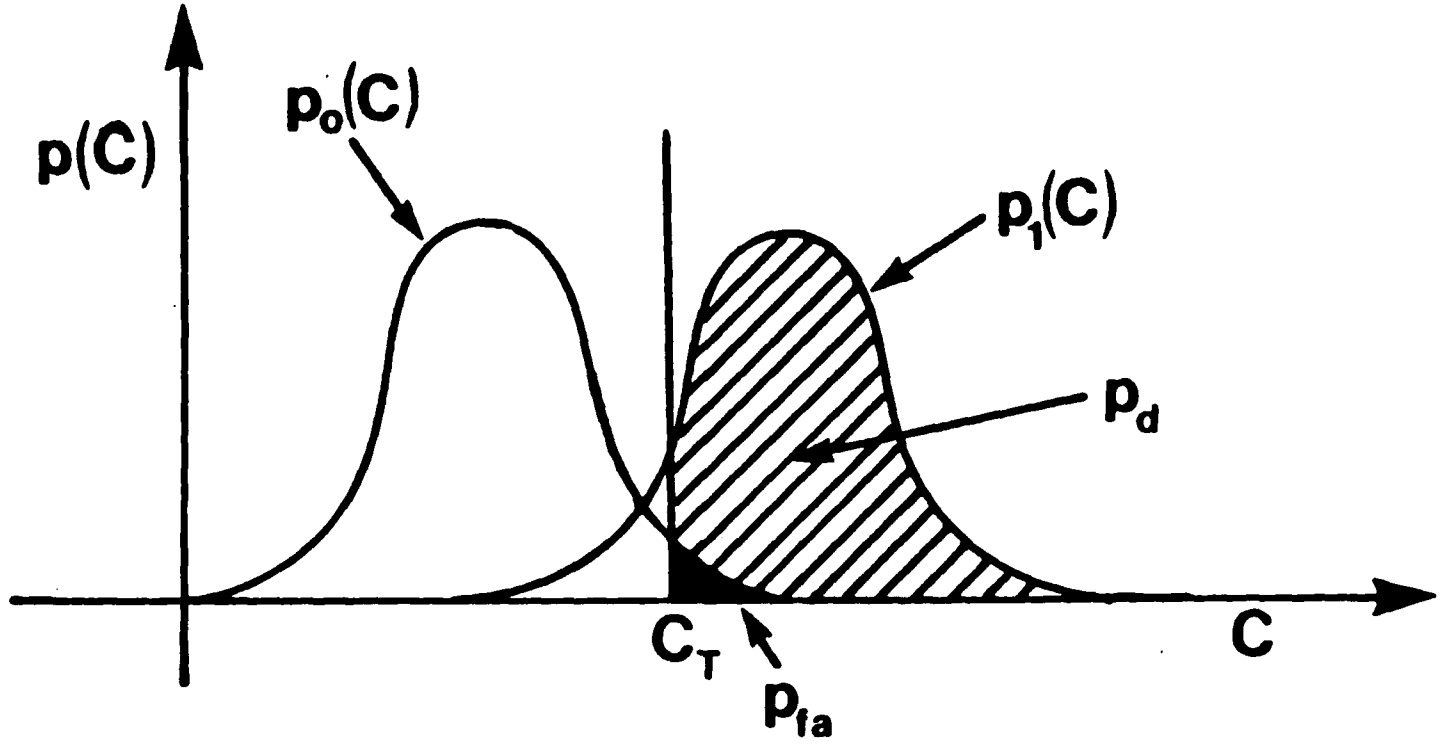

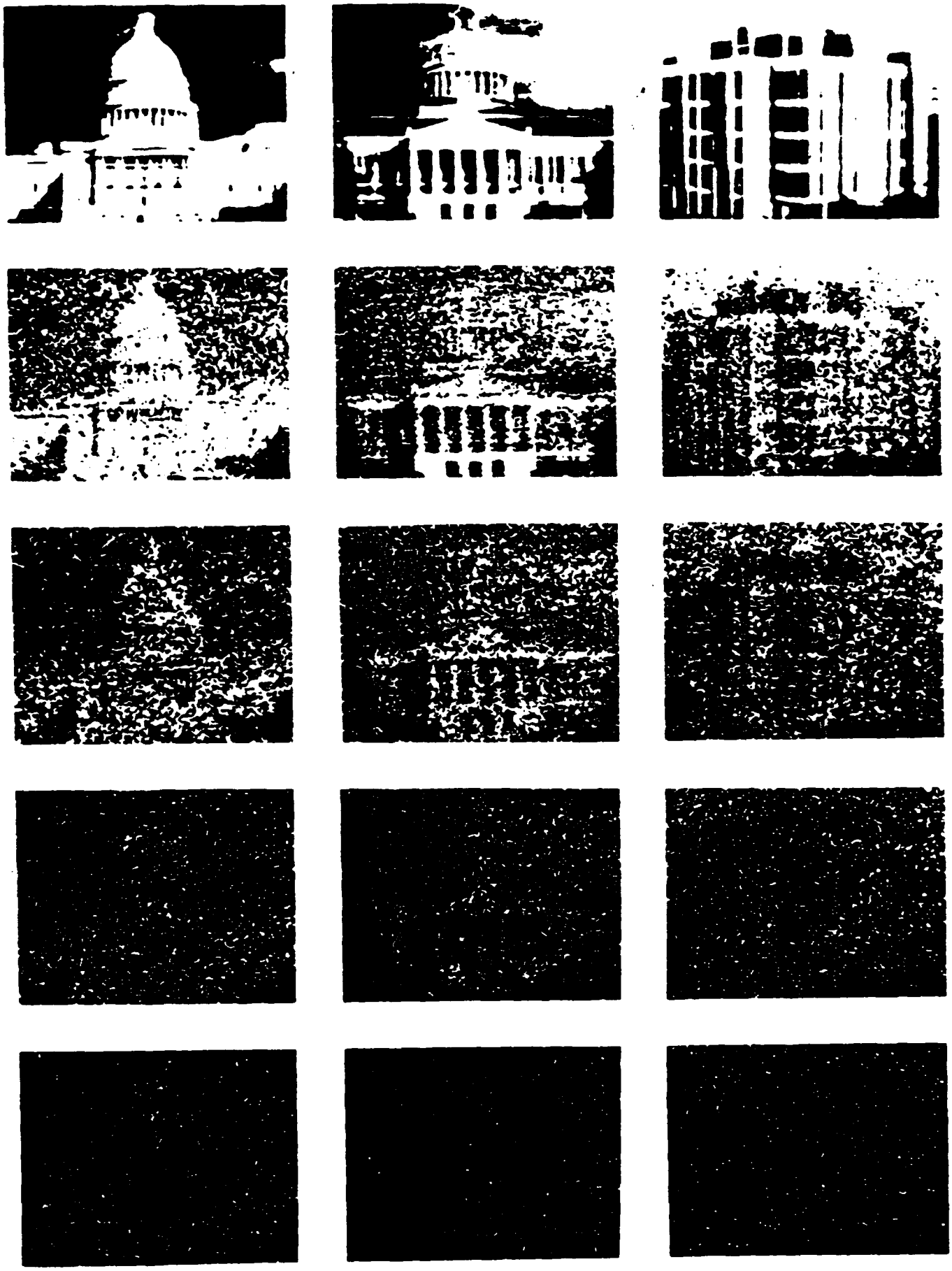
56 GRAY LEVELS
-16K
-4K
-1K
-250

PDF's – CORRELATION SIGNAL

REFERENCE: CAPITOL BLDG.

256 GRAY LEVELS

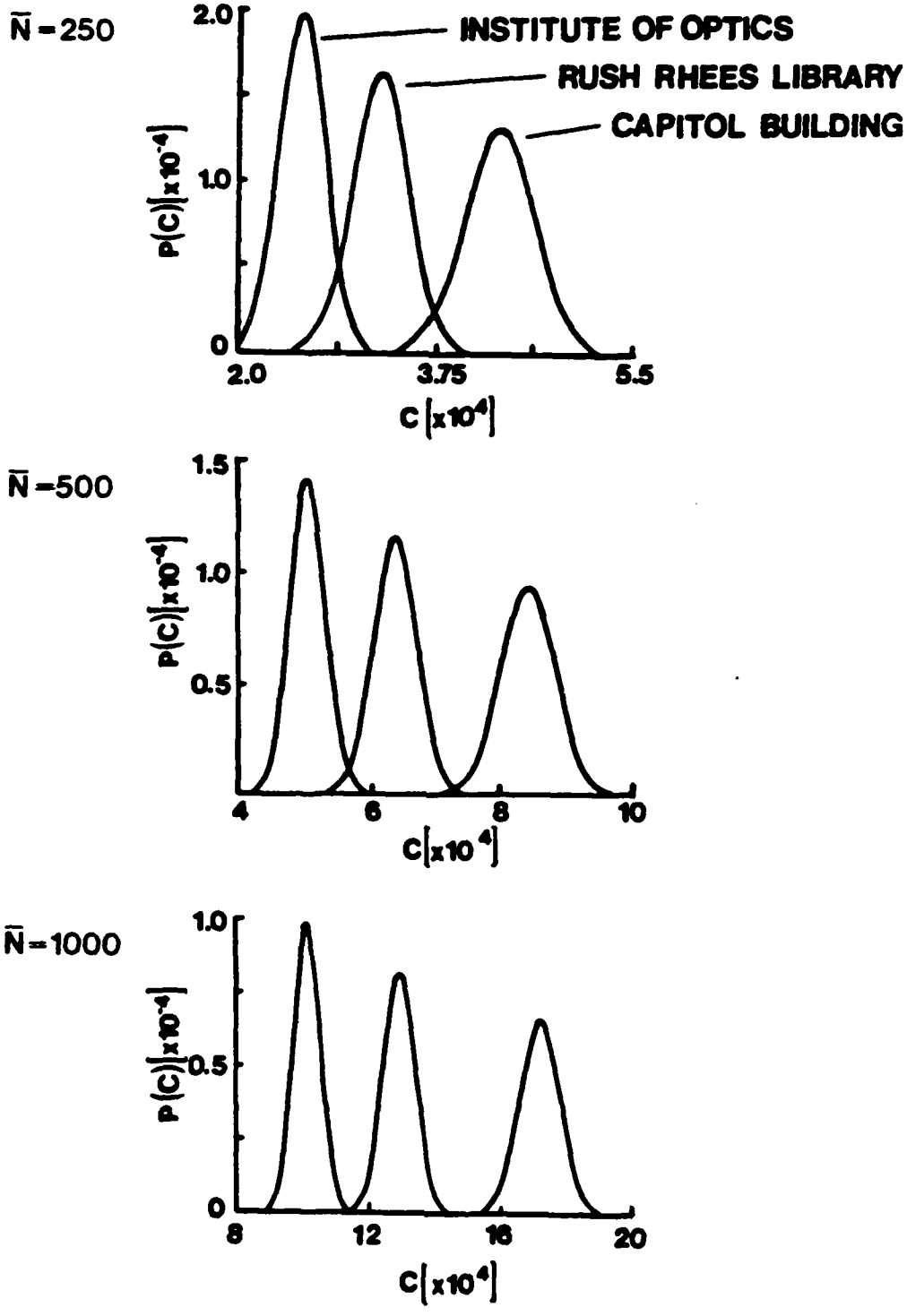

Distortion-Invariant Image Recognition

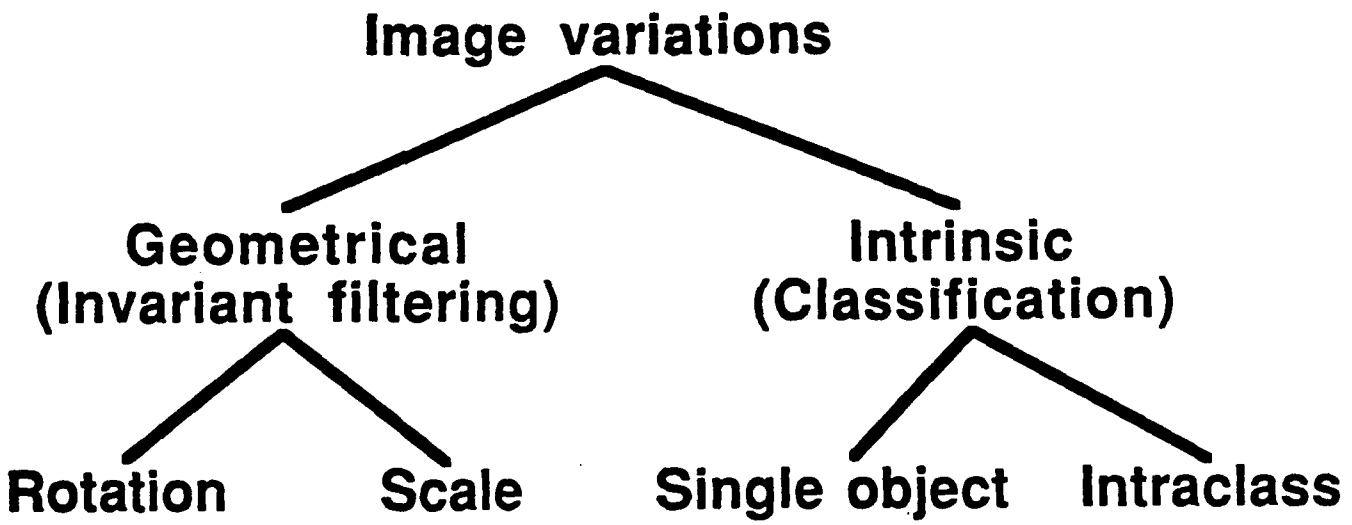

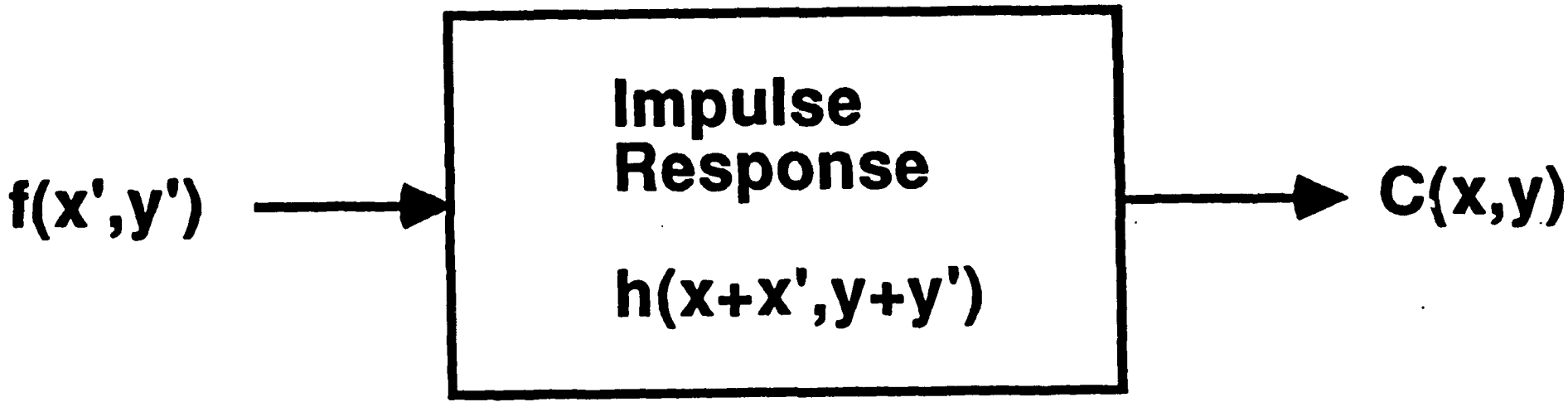
f(x',y')
Impulse
Response
h(x+x',y+y')
C(x,y)

CENTER FOR OPTO-ELECTRONIC SYSTEMS RESEARCH

INVARIANT FILTERING

Invariant Image Recognition using Quantum-Limited Images

Recognition of a Single Object within an Input Scene

- Rotation Invariant Filtering: Circular-Harmonic Filters
- Extraction of Rotation-, Position-, and Scale-Invariant features: Radial Moments of Circular-Harmonic Functions

Recognition of Multiple Objects within an Input Scene

- Two-Stage Template Matching
- Two-Stage Invariant Filtering and Feature Extraction

Future Applications

- Correlation Tracking

Invariant Filtering

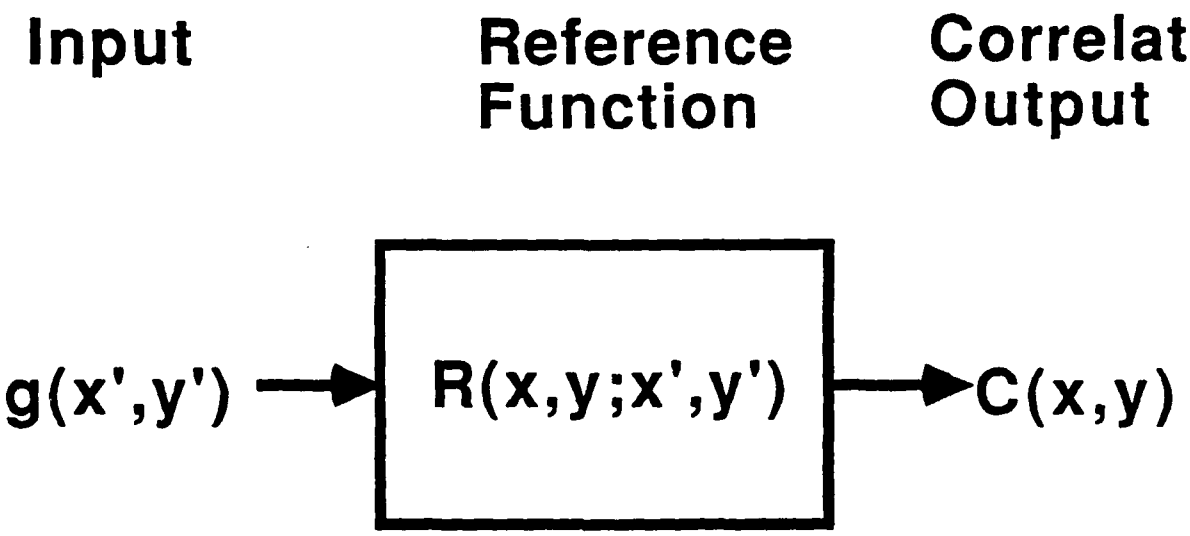

- C(x,y) remains unchanged when g(x',y') is rotated, scaled, or shifted.

- C(x,y) attains its maximum value when the reference object is input

Rotation-Invariance: The Circular-Harmonic Expansion

- **Expansion**

$$f(r,\theta) = \sum_{m=-\infty}^{\infty} F_m(r)\exp(im\theta)$$

where

$$F_m(r) = \frac{1}{2\pi}\int_0^{2\pi} f(r,\theta)\exp(-im\theta)d\theta$$

- **Reference function:** *mth harmonic*

$$F_m^*(r,\theta) = F_m^*(r)\exp(-im\theta)$$

- **Rotation-invariant correlation output**

$$|C(\alpha)| = |(g(r,\theta+\alpha),F_m^*(r,\theta))|$$

$$= |e^{im\alpha}\int_0^{\infty} G_m(r)\,F_m^*(r)\,r\,dr\,|$$

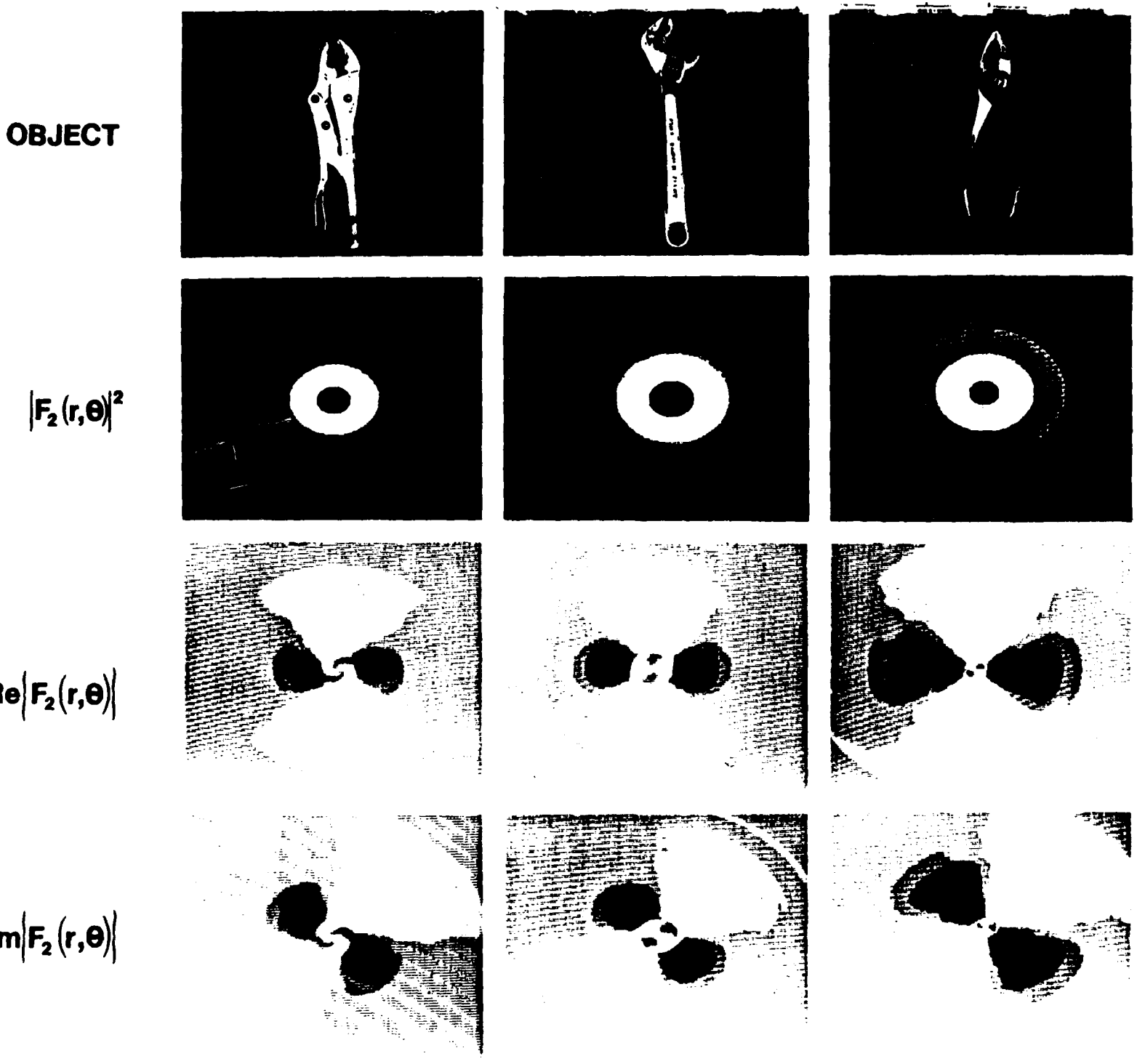
OBJECT
$|F_2(r,\theta)|^2$
$\mathrm{Re}|F_2(r,\theta)|$
$\mathrm{Im}|F_2(r,\theta)|$

DETERMINATION OF ROTATION ANGLE

REF. OBJECT : VISE GRIPS

N=3000

MEAN : 89.6°

Std. Dev.: 0.705°

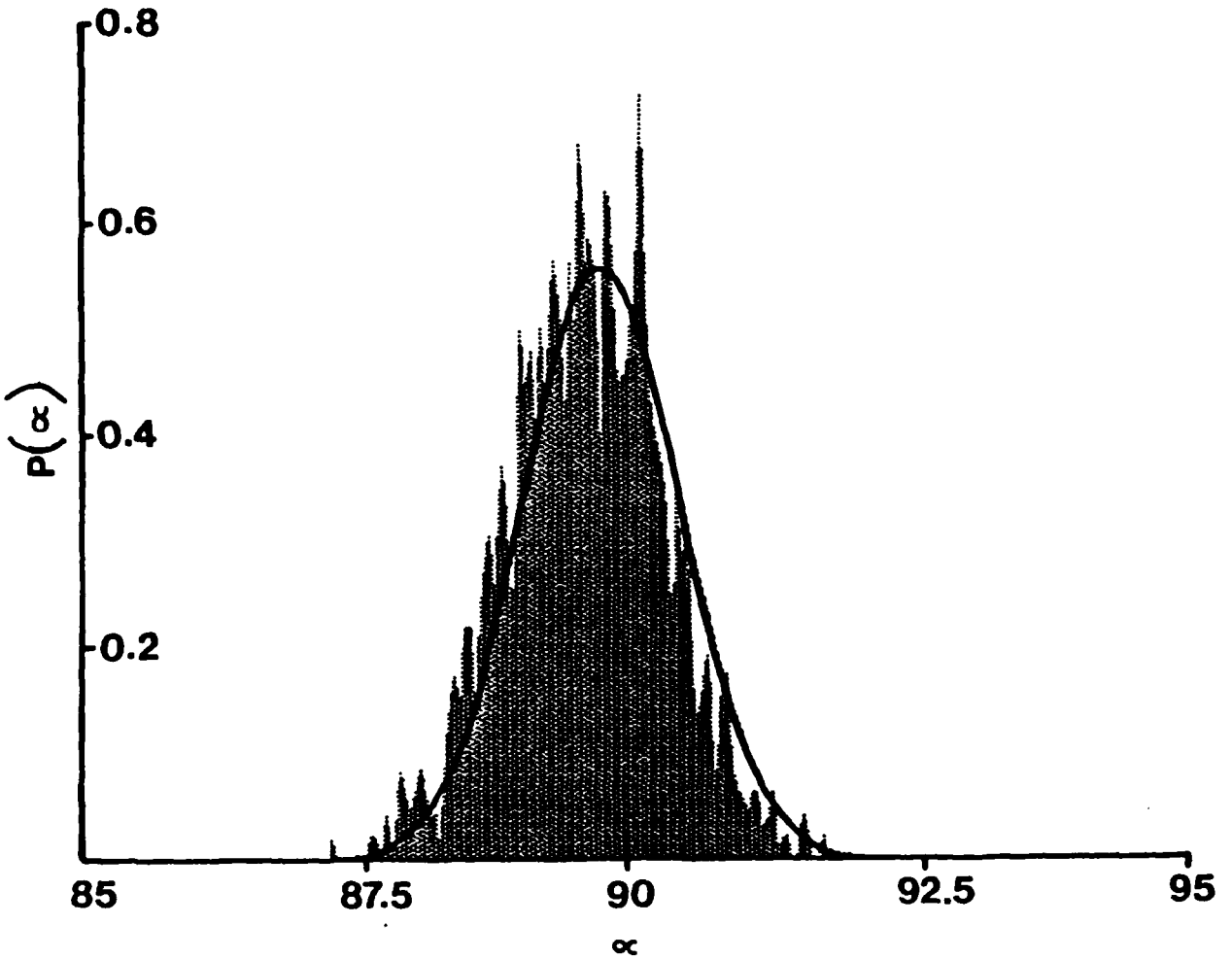

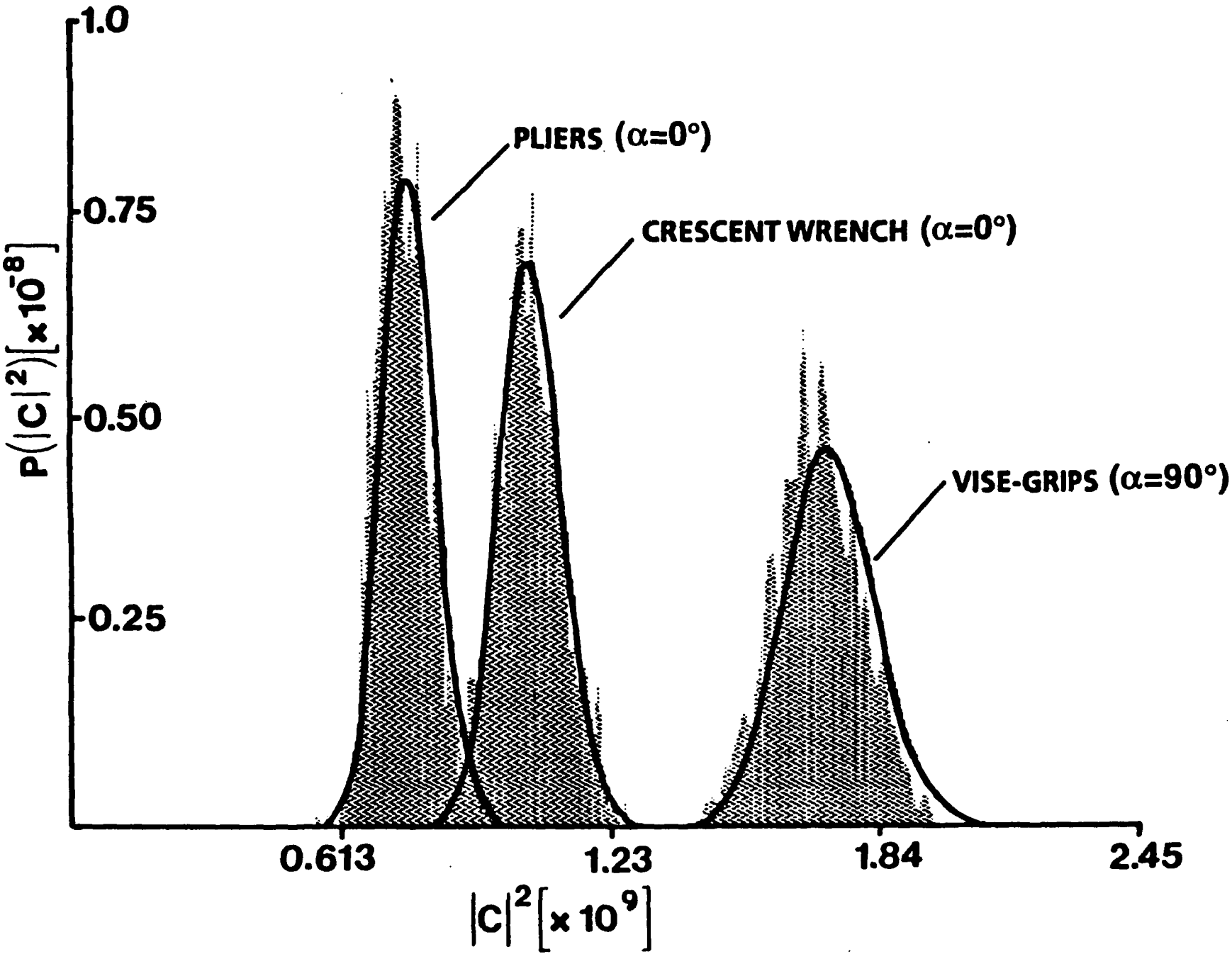
1.0
0.75
0.50
0.25
P(|C|²)[×10⁻⁸]
PLIERS (α=0°)
CRESCENT WRENCH (α=0°)
VISE-GRIPS (α=90°)
0.613
1.23
1.84
2.45
|C|²[×10⁹]

Radial Moments of Circular-Harmonic Functions†

$$M_{s,m} = \int_0^{2\pi} \int_0^{\infty} r^{s-1} e^{-im\theta} f(\gamma r, \theta + \alpha)\, dr d\theta$$

$$= \gamma^{-s} e^{im\alpha} \int_0^{2\pi} \int_0^{\infty} r^{s-1} e^{-im\theta} f(r,\theta) dr d\theta$$

Invariant Feature $\Phi_{s,m}$:

$$\Phi_{s,m} = \frac{|M_{s,m}|}{|M_{s,0}|}$$

Decision Criterion: Distance in Feature Space, D

$$D = \sum_m \left(\Phi_{s,m}^{(inp)} - \Phi_{s,m}^{(ref)} \right)^2$$

†Ref: Sheng and Arsenault, JOSA A 3, 771 (1986).

Photon-Limited Estimation of Radial Moments of CHF's

Ref. Function: $r^{s-2} e^{-im\theta}$

Choose s = 2

$$\langle C \rangle = \frac{N \int_0^{2\pi} \int_0^{\infty} f(r,\theta)\, e^{-im\theta}\, r\,dr\,d\theta}{\int_0^{2\pi} \int_0^{\infty} f(r,\theta)\, r\,dr\,d\theta}$$

$$\frac{|\langle C \rangle|}{N} = \frac{|M_{2,m}|}{|M_{2,0}|} = \Phi_{2,m}$$

Invariant Image Recogniton

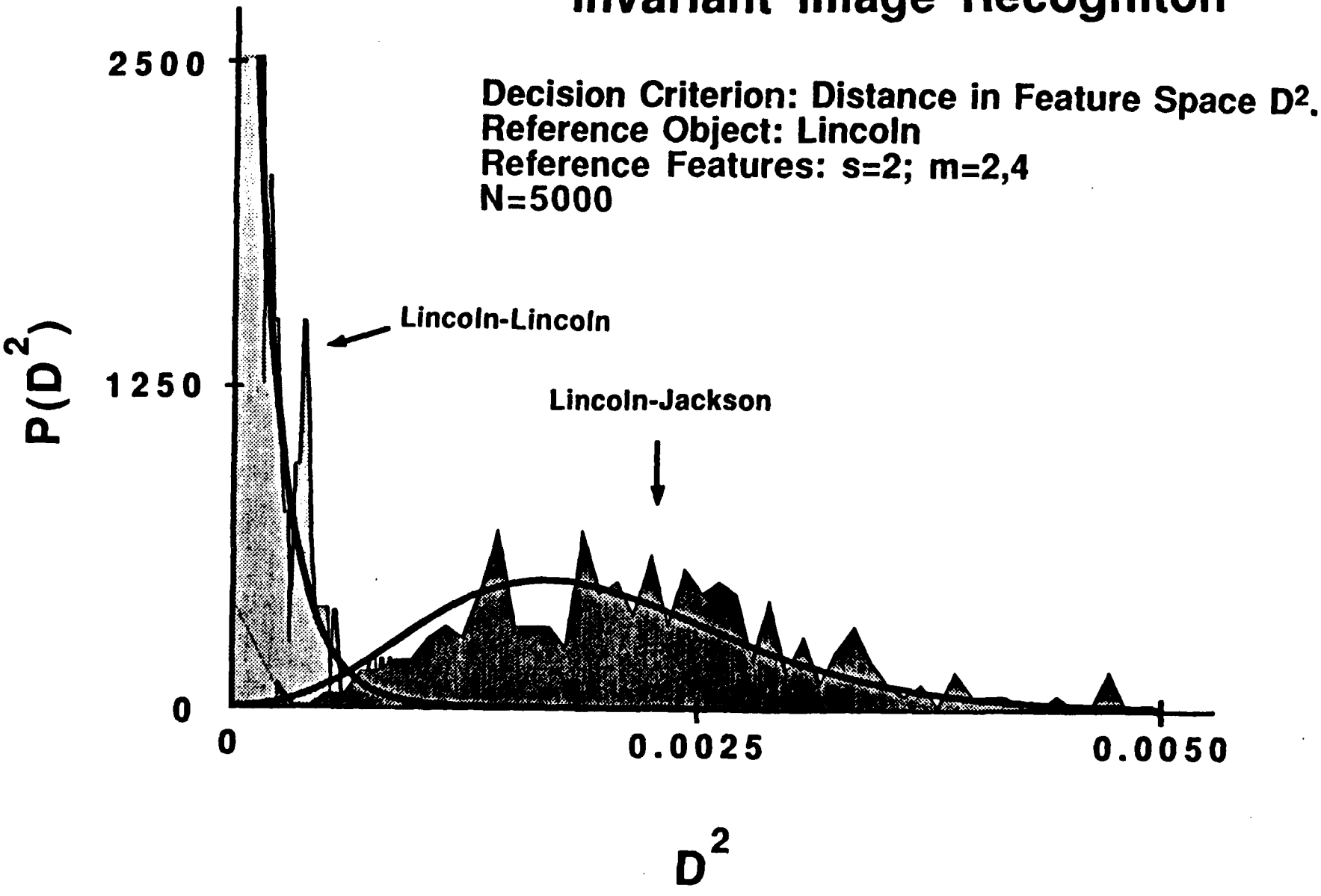

Invariant Image Recogniton

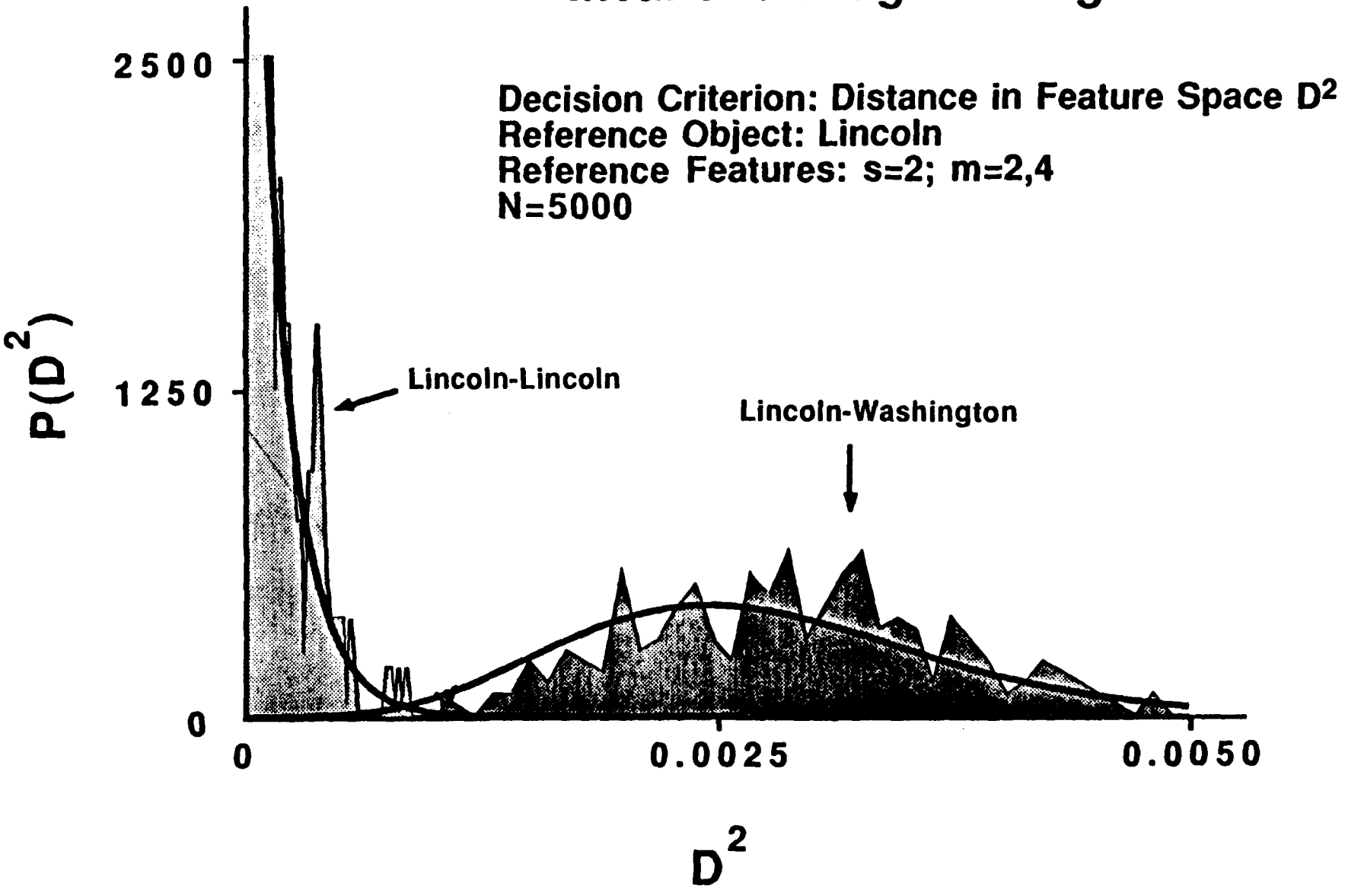

Two-Stage Template Matching

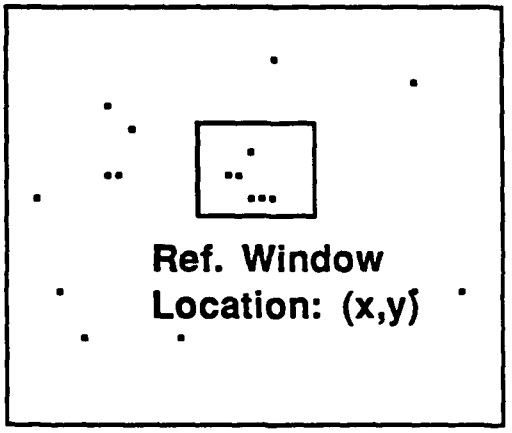

Before Implementation:

1. Specify required probabilites of detection and false alarm.

2. Choose similarity criterion and number of photons for each stage.

Stage One

- Move the location of the ref. window to each point in the input scene.
- Sample using a small number of detected photons.
- Compute correlation function or invariant features.
- Apply threshold similarity criterion.

Stage Two

- Examine the locations that satisfied the similarity criterion using a sufficient number of photons to achieve the specified probabilities of detection and false alarm.

Two-Stage Template Matching

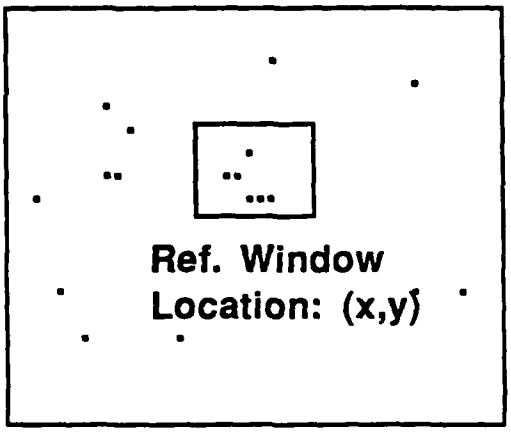

Determination of the number of photons and similarity criterion for each stage:

- The number of photons in the first stage should be as small as possible.
- The similarity criterion is chosen to achieve the required probability of detection, while allowing as few false alarms as possible.
- The number of photons and similarity criterion in the second stage are chosen such that the false alarms from the first stage are eliminated.
- For a given input scene, it is possible to optimize the choice for the similarity criterion and number of photons in each stage.

Two-Stage Template Matching

Reference Object: Tape Dispenser

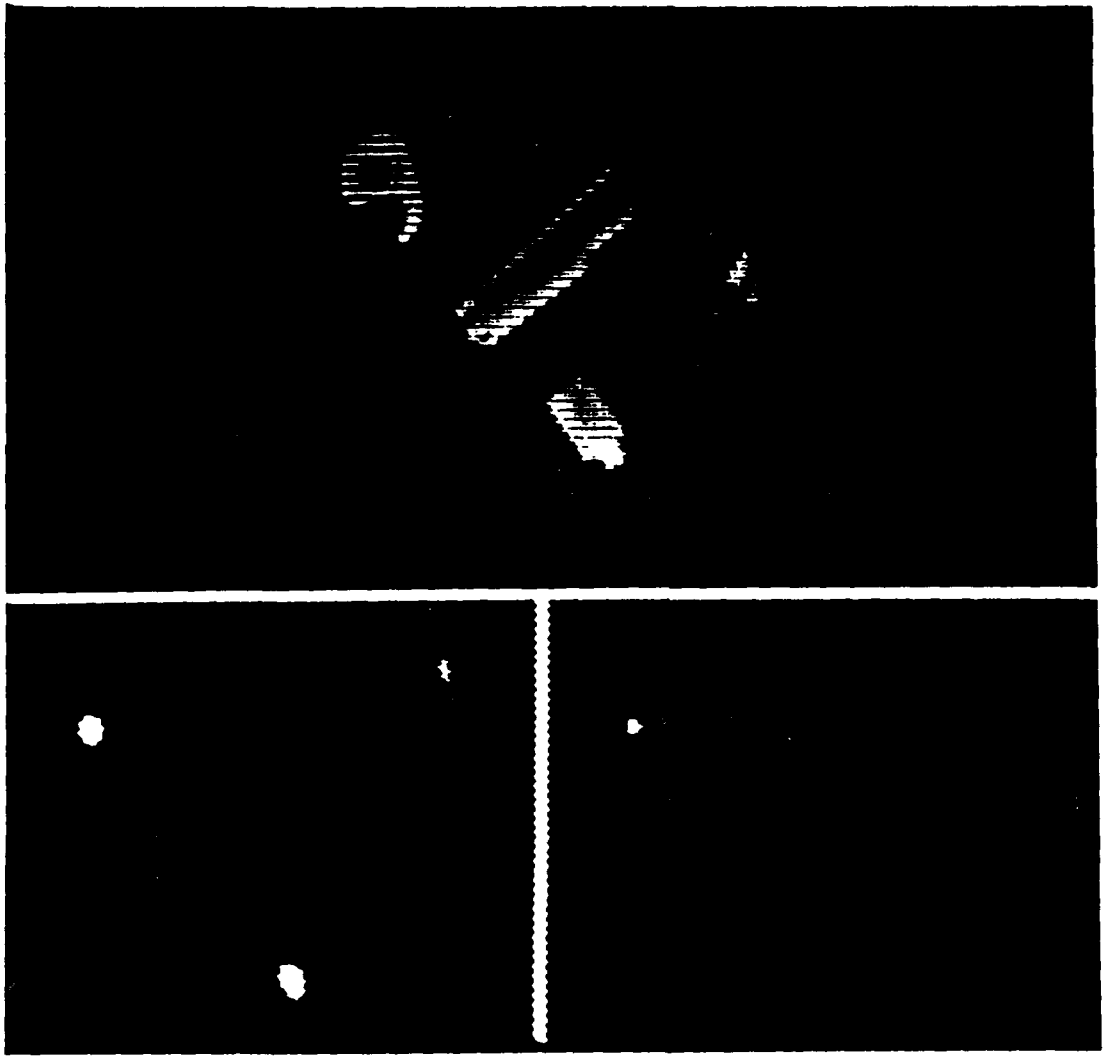

Stage 1

N=15

Stage 2

N=100

Probability that the similarity criterion will be satisfied at each window offset.

CENTER FOR OPTO-ELECTRONIC SYSTEMS RESEARCH

IMAGE CLASSIFICATION

Maximum-Likelihood Image Classification

- The role of the classifier
- The maximum-likelihood approach
- Related strategies
- The maximum-likelihood filter
- Results
- Implementation

The ML approach

- **Log-likelihood ratio**

$$\ln\{l(\underline{n})\} = \ln\left\{\frac{p[\,\underline{n} \mid H^{(1)}]}{p[\,\underline{n} \mid H^{(2)}]}\right\}$$

- **Decision rule**

$$\ln\{l(\underline{n})\} \underset{d_2}{\overset{d_1}{\gtrless}} 0$$

Related strategies

- **Minimize probability of error**

$$\ln\{l(\underline{n})\} \underset{d_2}{\overset{d_1}{\gtrless}} \ln\left\{\frac{p[H^{(2)}]}{p[H^{(1)}]}\right\}$$

- **Minimize cost of decision**

$$\ln\{l(\underline{n})\} \underset{d_2}{\overset{d_1}{\gtrless}} \ln\left\{\frac{(c_{12} - c_{22})p[H^{(2)}]}{(c_{21} - c_{11})p[H^{(1)}]}\right\}$$

where $p(H^{(j)})$ = *a priori*, class j

c_{ij} = cost of deciding i when j is correct

The Maximum-Likelihood Filter*

$$\ln\{l(\underline{n})\} \cong \sum_i n_i \ln\{\frac{m_{1,i}}{m_{2,i}}\}$$

$\underline{m}_j$ = average image for class j

Multinomial or Poisson statistics
Assume small intraclass variations

* JOSA A, 3, 2179 (1986).

(a)

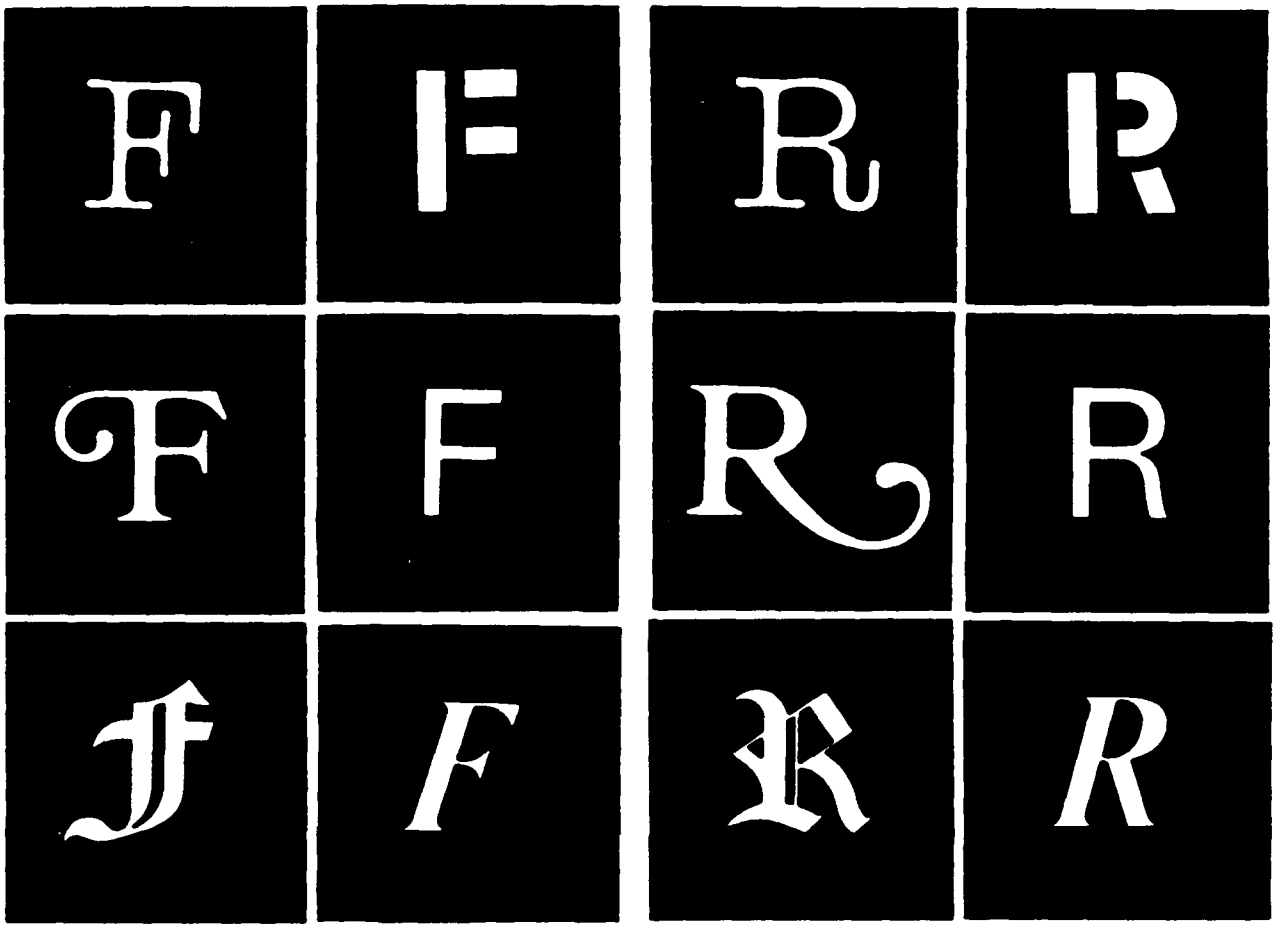

(b)

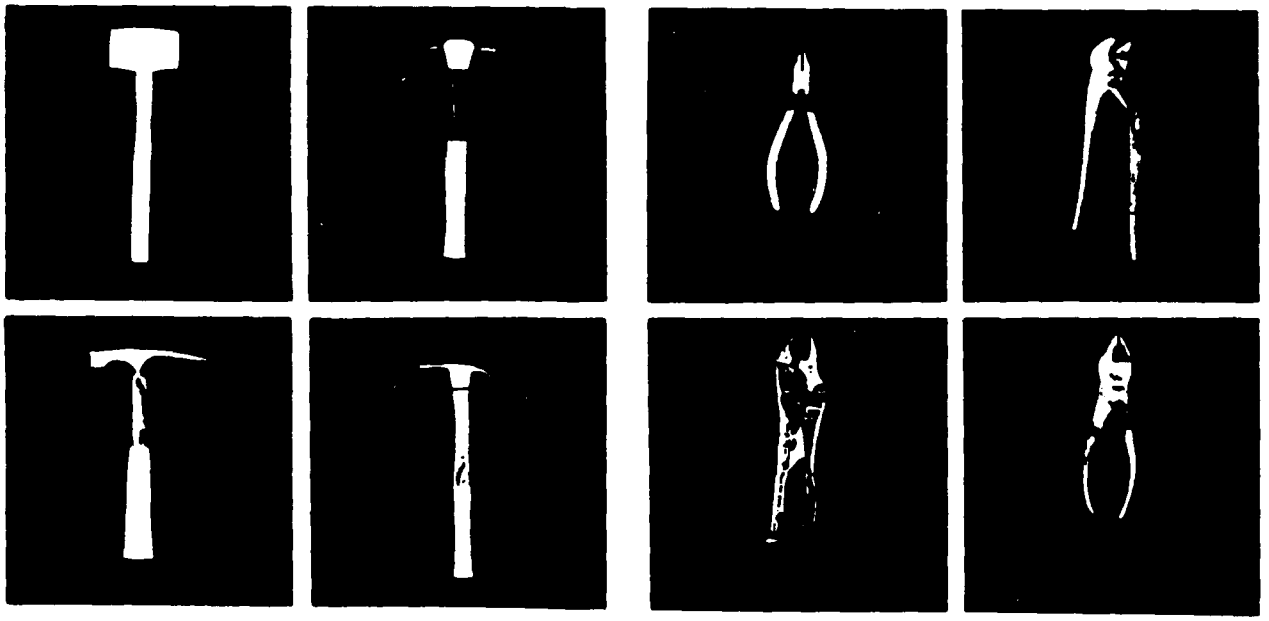

Reference Function for Maximum-Likelihood Classification

$$R(x,y) = \ln\left\{\frac{m_1(x,y)}{m_2(x,y)}\right\}$$

$m_1(x,y)$ = mean of class 1
$m_2(x,y)$ = mean of class 2

Summary of results

(number of detected photoevents to achieve 1/10000 error rate)

Tools

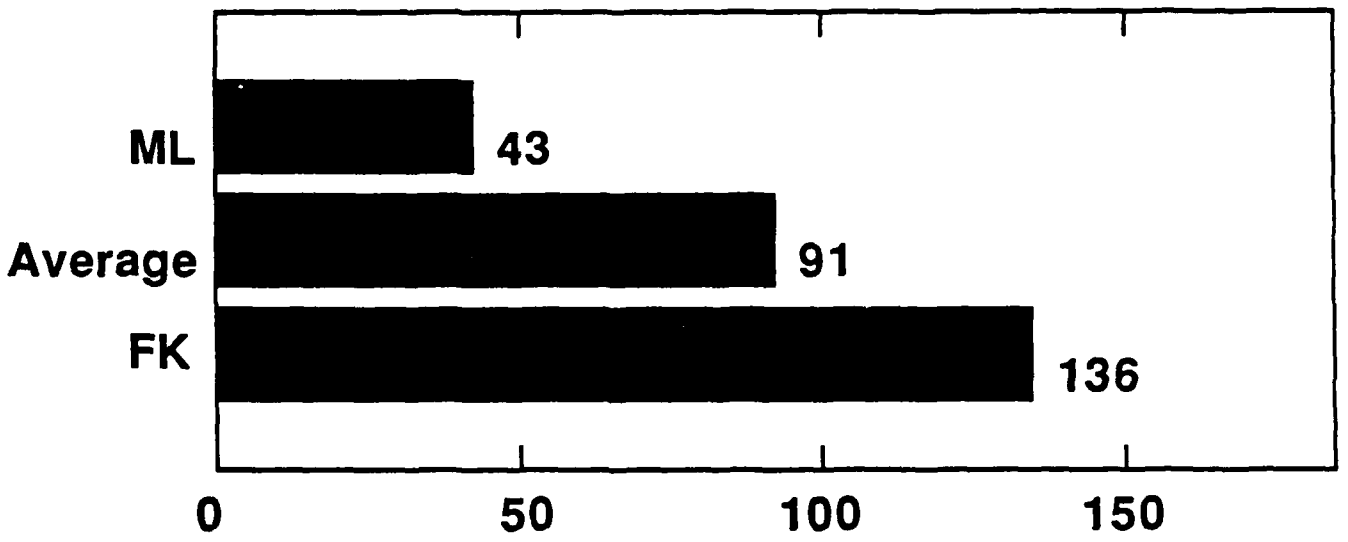

Characters

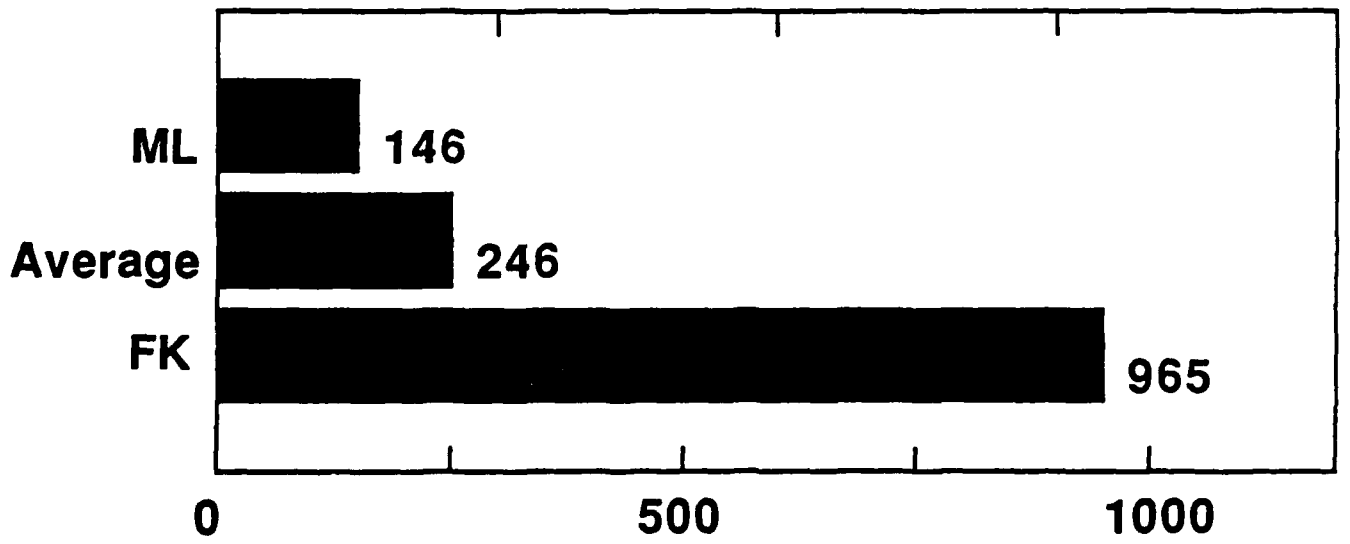

Optical Implementation

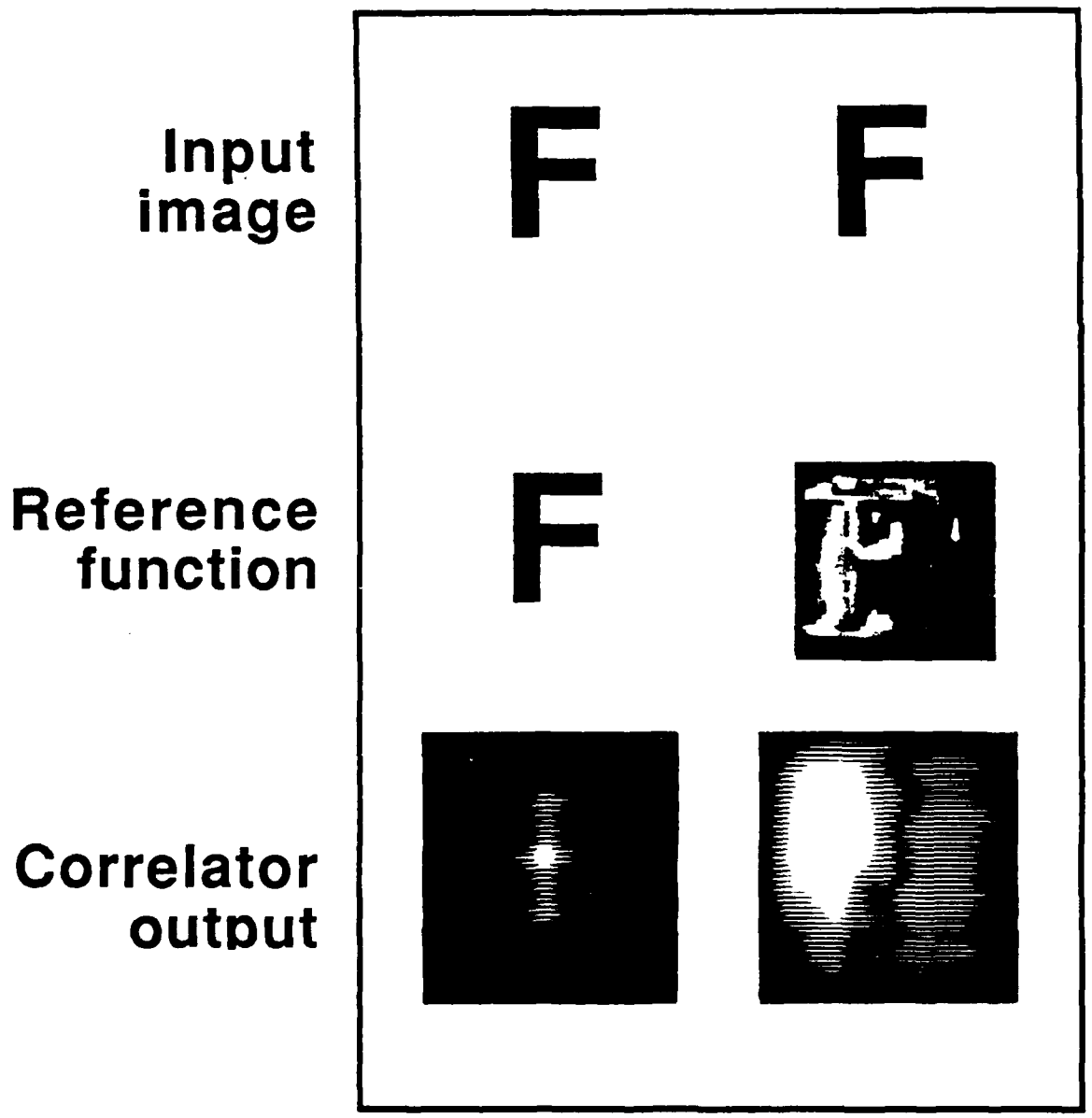

Filter Representations

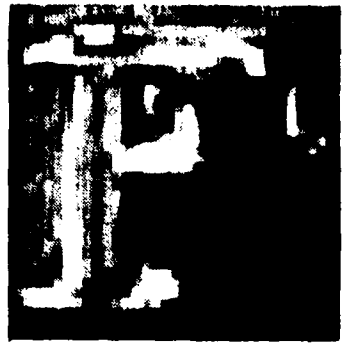

$\ln\{\underline{m}_1/\underline{m}_2\}$

$\ln\{\underline{m}_1\} - \ln\{\underline{m}_2\}$

Classification Results (F vs. R)

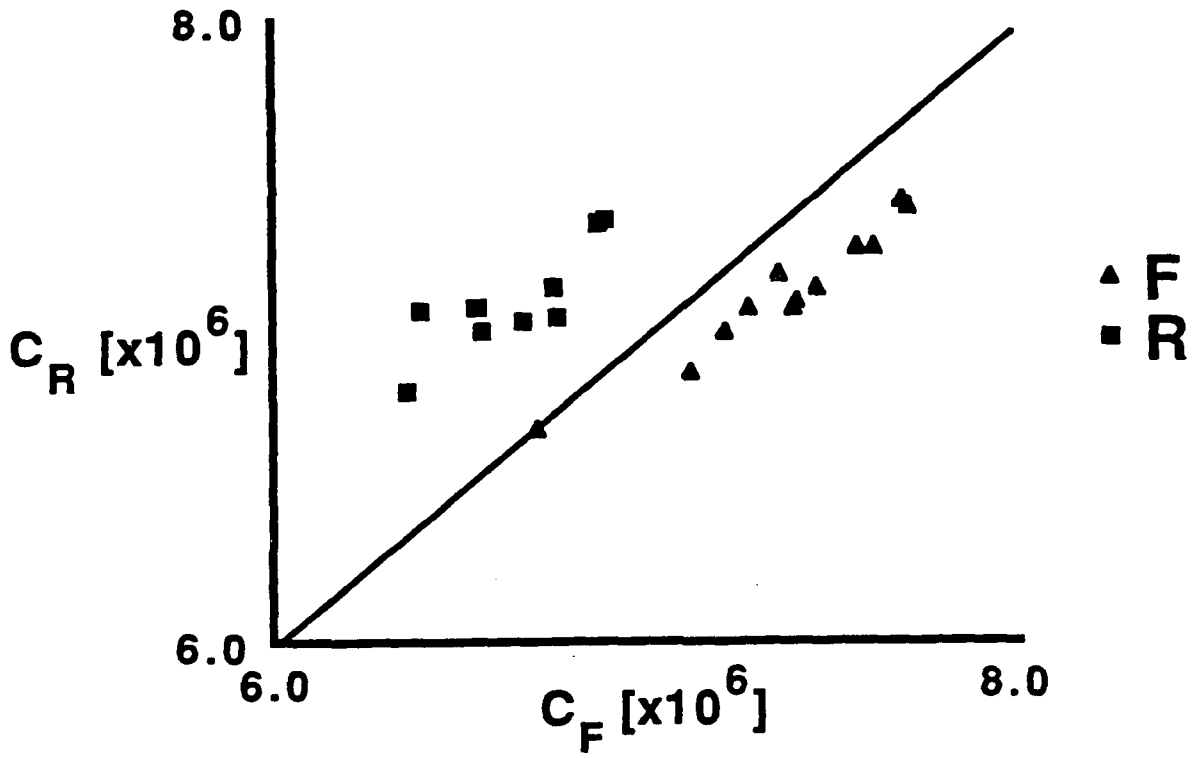

MSLM-based optical correlator configuration

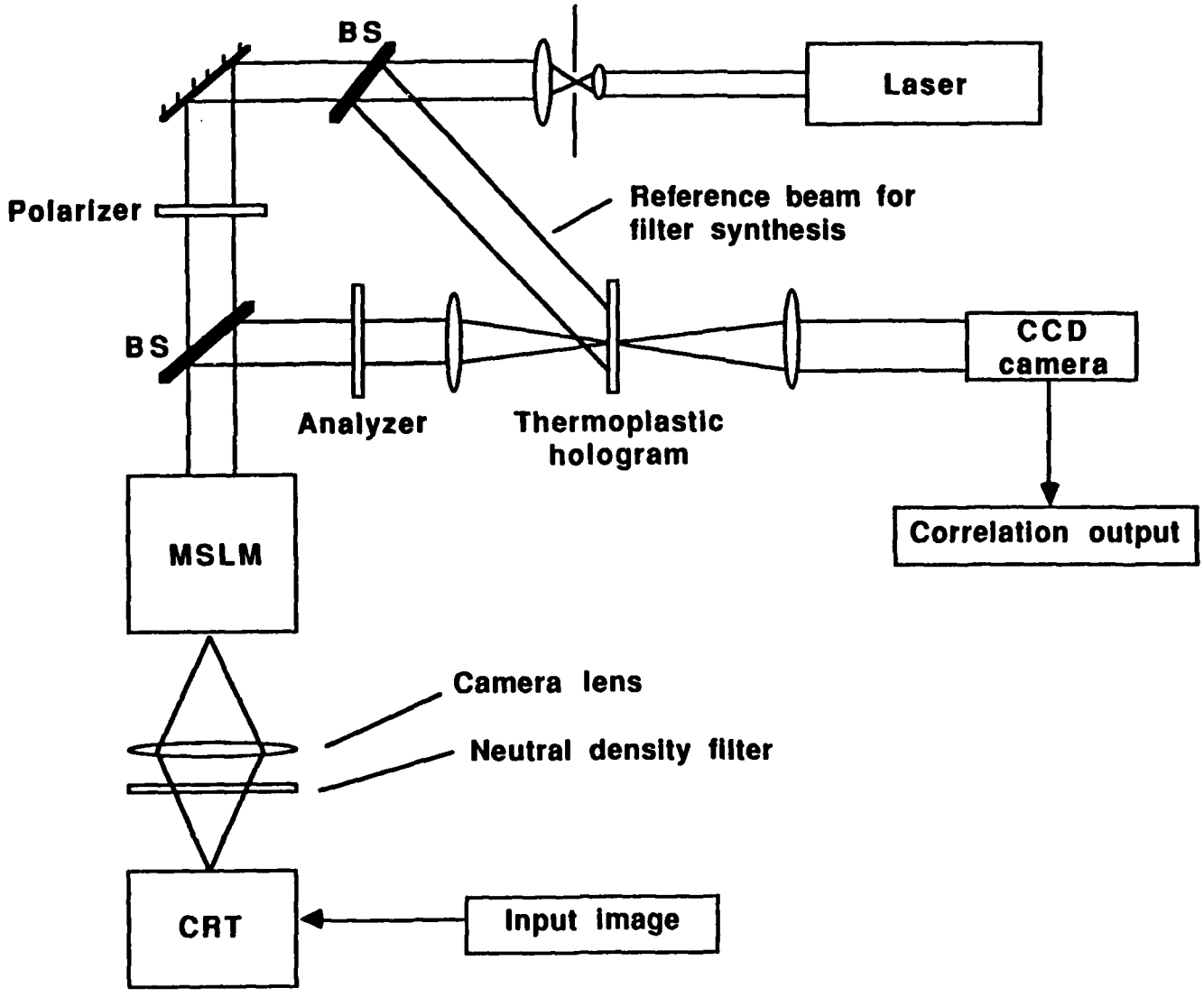

Summary

- Intraclass or single object variations
- Linear filter solution
- Many strategies can be implemented
- Successful classification results
- Optical correlator implementation

CENTER FOR OPTO-ELECTRONIC SYSTEMS RESEARCH

UPCONVERSION OF BROADBAND INFRARED IMAGES

Quantum-Limited Imaging of Upconverted Infrared Radiation

Outline

- Quantum-limited infrared detection
- Upconversion methods
- Narrow band imaging
- Broadband imaging
- Broadband upconversion
- Upconversion systems
- Summary

Infrared Detection

Current detector technology

- Low number of pixels
- Requires cooling
- No mature methods for doing photon-counting

Visible images by IR upconversion

- Allows use of well-developed visible detection
- Large space-bandwidth product
- Uncooled
- Photon-counting capability

Upconversion Methods

Incoherent (Bloembergen, 1959)

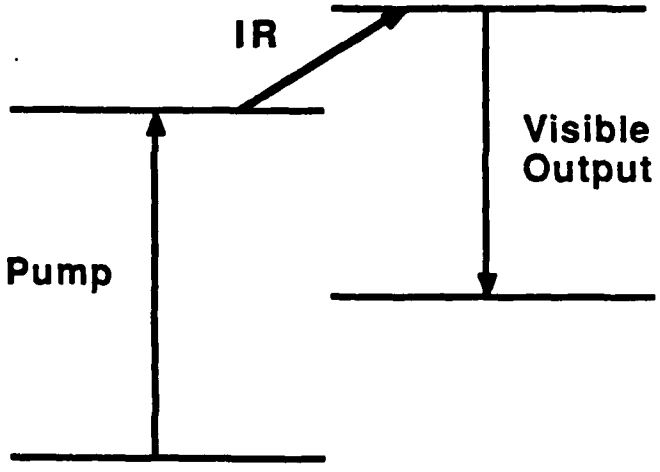

- No coherence requirement on pump.
- Narrow band (limited to bandwidth of IR transition)

Coherent (Armstrong et al, 1962)

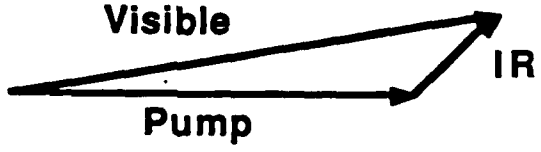

Phase matching

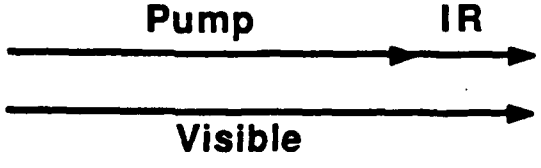

Energy matching

- Only phased-matched IR efficiently upconverts
- Limited bandwidth

Narrow Band Imaging

Large D*

- Active illumination is narrow band
- Noise is broad band

Range extension/increased resolution by photon-counting

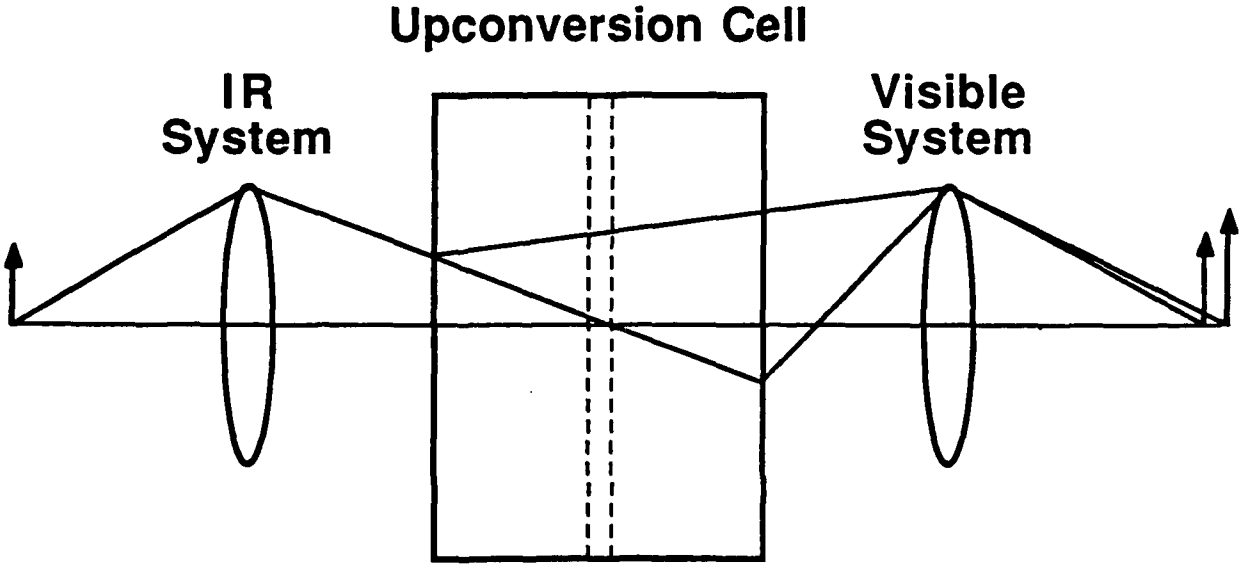

Broadband Imaging

Classical intensity levels

Broadband imaging improves performance

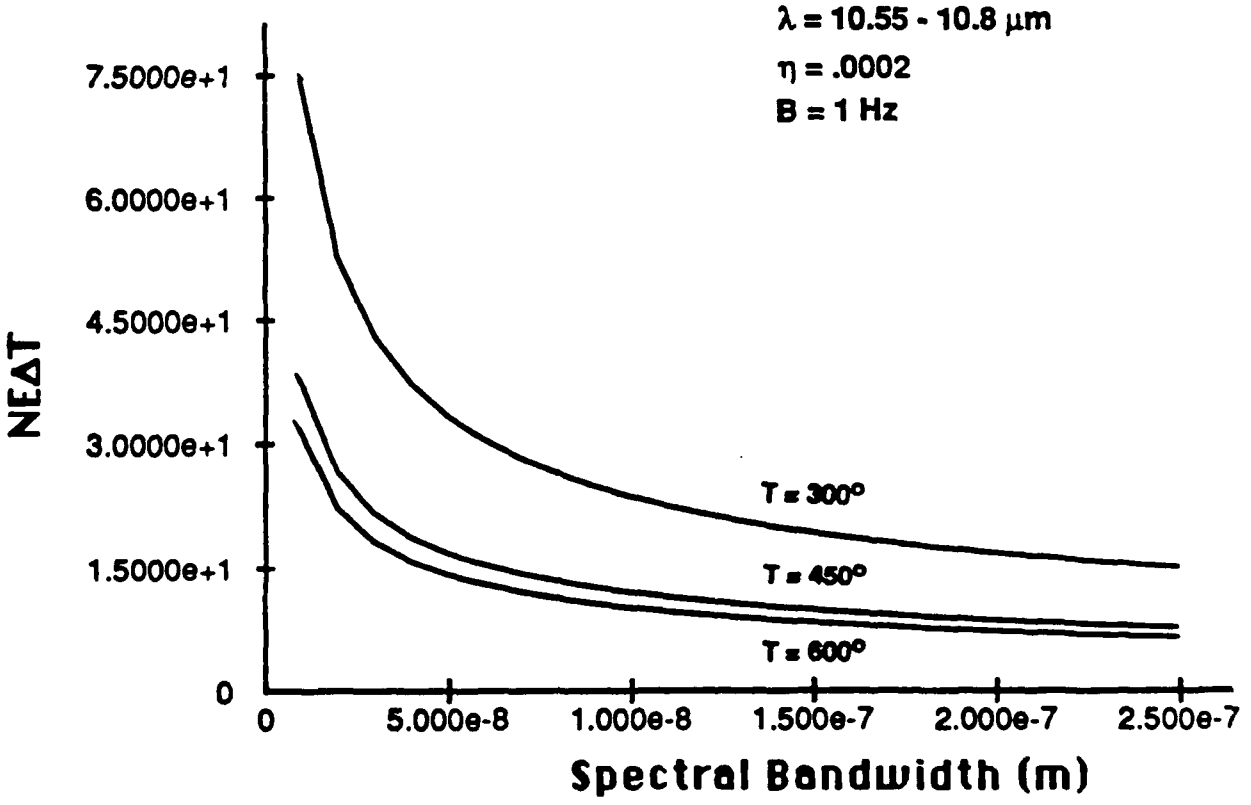

Broadband Upconversion

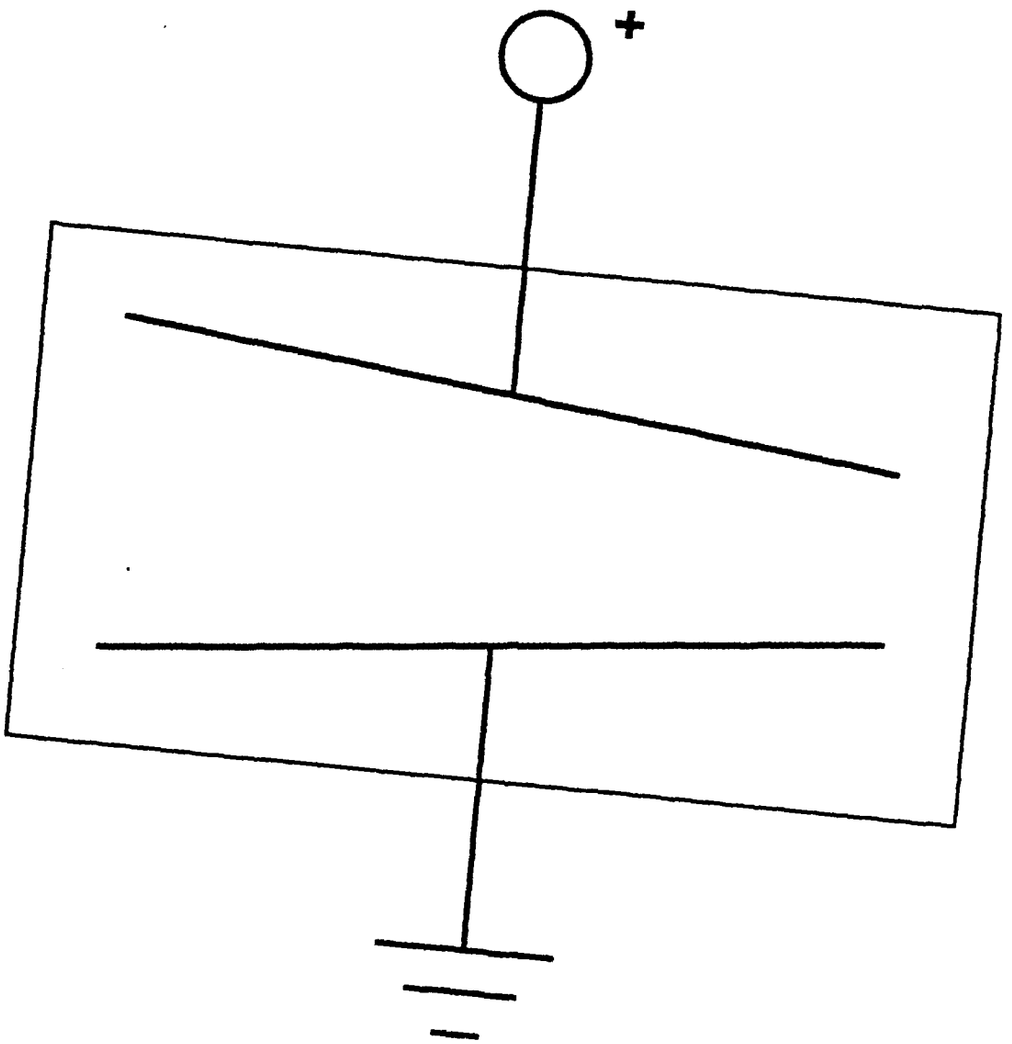

Alkali - metal vapor allows Stark tuning

Tilted plates produces variable Stark shift along axis of cell

Incoherent Broadband Upconversion

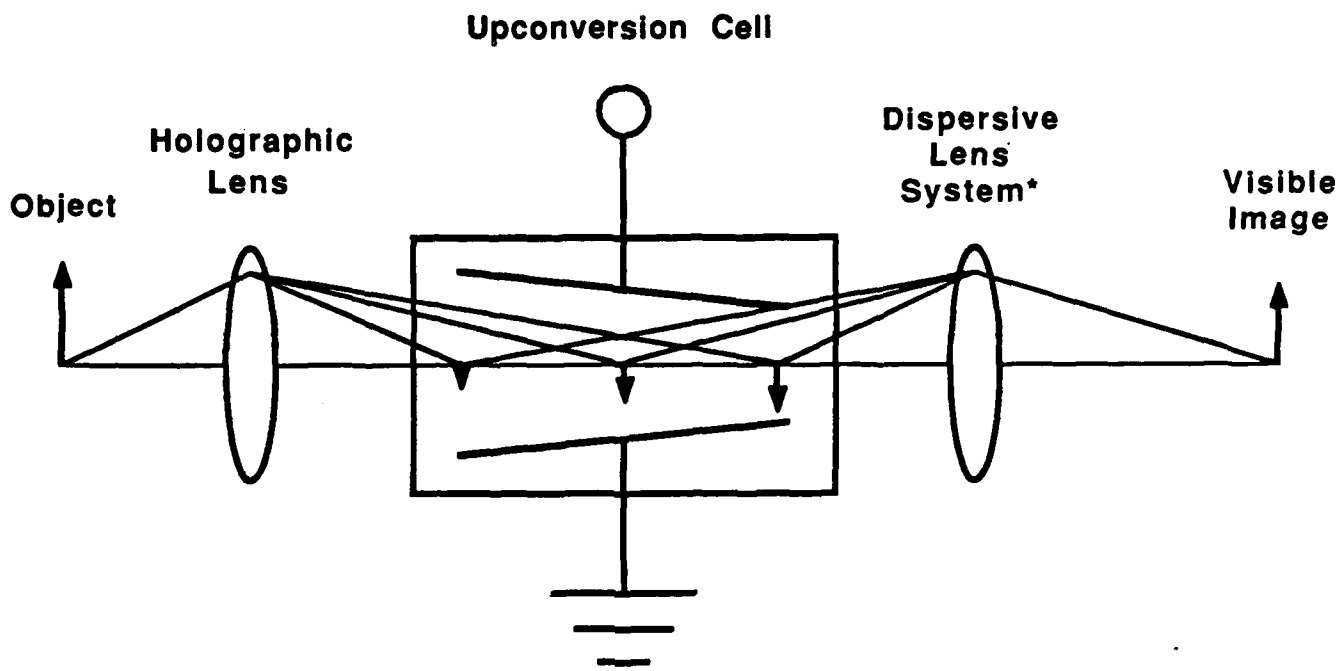

Dispersive element spreads image in upconversion cell

Each wavelength upconverts at different point in cell

Final dispersive lens system recombines visible light into single image

*D. Faklis and G. M. Morris, "Broadband Imaging with Holographic Lenses," submitted to Applied Optics, in review.

Coherent Broadband Upconversion

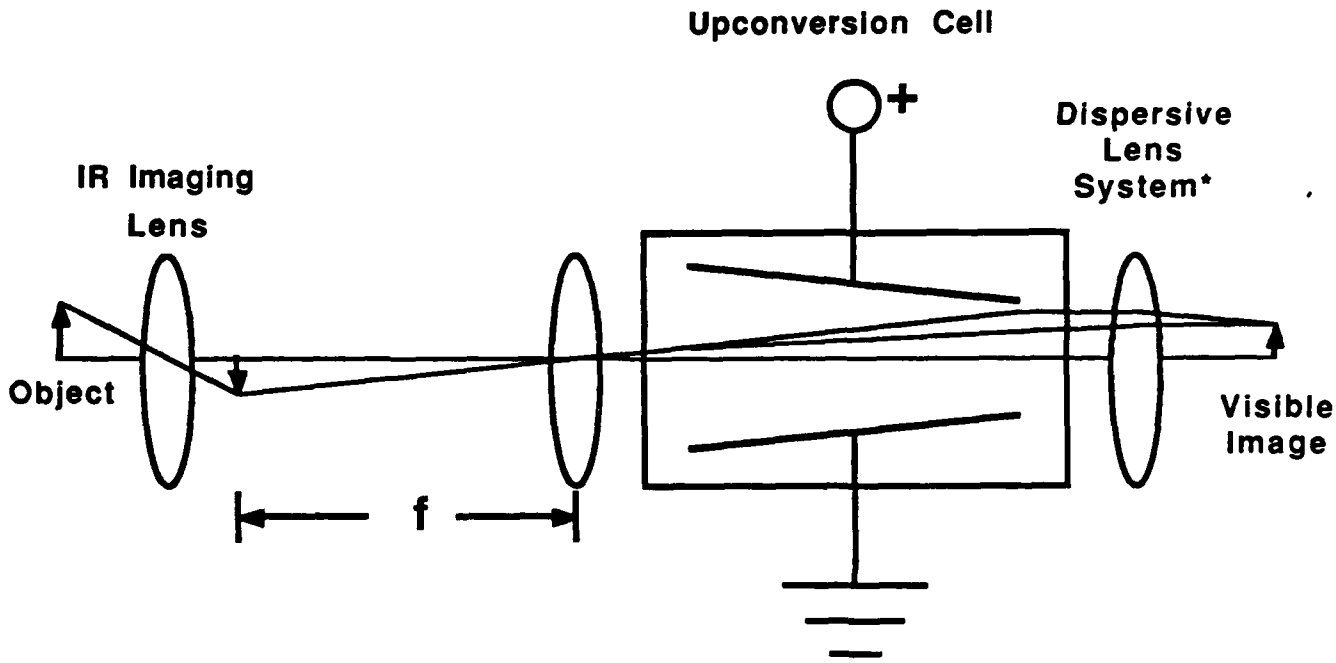

Second lens produces plane waves in cell

Each wavelength upconverts at different point, producing a plane wave

Final dispersive element forms single image

G. M. Morris and D. A. Zweig, "White-Light Fourier Transformations," In Optical Signal Processing, (J. Horner ed.), pp 23-71, Academic Press, New York (1987).

Summary

Advantages of upconversion

- Larger number of pixels than direct IR imaging
- Uncooled
- Photon-counting capability

Active imaging uses narrow band, photon-counting upconversion

Passive imaging requires broadband upconversion

- Dispersive optical elements
- Alkali-metal vapor cells

Monte Carlo Image Compression and Computing Systems

Low-Light-Level Implementation

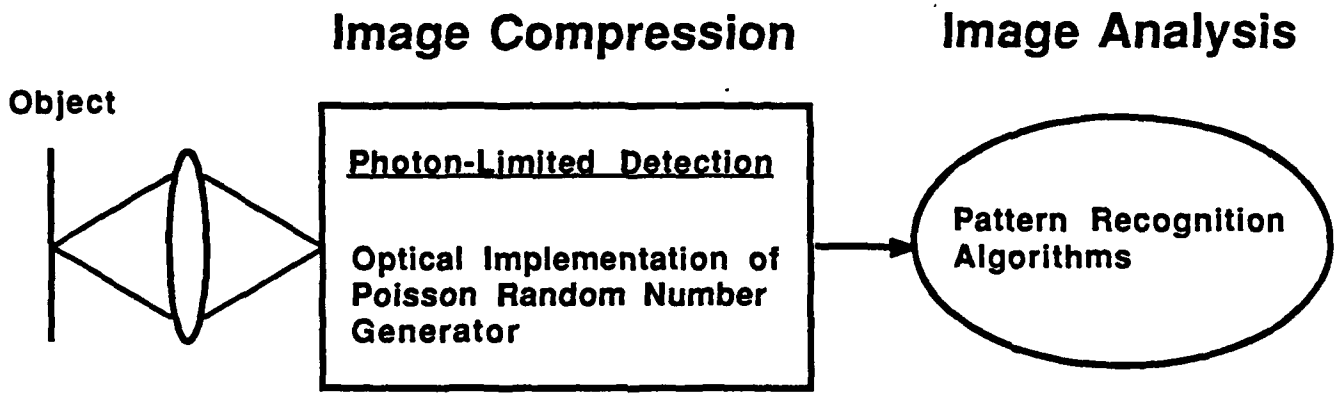

Electronic Implementation

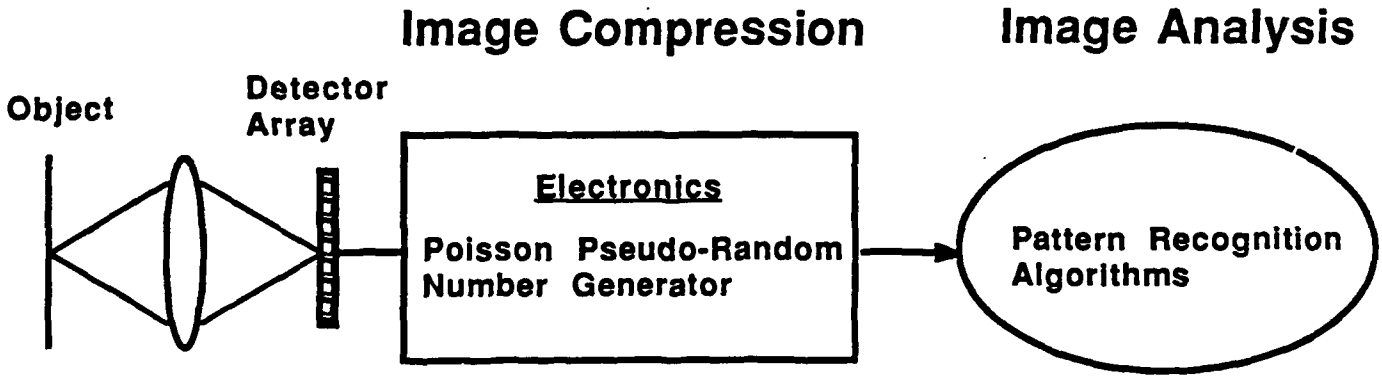

Pattern Recognition using Quantum-Limited Images

Features

- Data Reduction and Computation Speed
- Minimal Computing Hardware
- Intensity-Based System

Potential Applications

Machine and Robot Vision
Automatic Target Recognition
    Low light levels (passive night vision)
    Laser radar systems
Correlation Tracker for Vehicle Guidance
Recognition of Spectroscopic Signatures
Radiological and Nuclear Imaging

CENTER FOR OPTO-ELECTRONIC SYSTEMS RESEARCH
SUMMARY

Industrial Applications", Proc. SPIE
Vol. 960, Dearborn, MI, June 27-28, 1988

Pattern Recognition using Photon-Limited Images

G. Michael Morris, Thomas A. Isberg, and Miles N. Wernick

The Institute of Optics, University of Rochester
Rochester, New York 14627

ABSTRACT

The spatial coordinates of detected photoevents and the number of detected photoevents in a given area convey information about the classical irradiance of the input scene. In this paper the effectiveness of photon-counting techniques for image recognition is discussed. A correlation signal is obtained by cross correlating a photon-limited input scene with a classical intensity reference function stored in computer memory. Laboratory experiments involving matched filtering, rotation- and scale-invariant image recognition, and image classification are reported. For many images it is found that only a sparse sampling of the input is required to obtain accurate recognition decisions, and the digital processing of the data is extremely efficient. Using available photon-counting detection systems, the total time required to detect, process, and make a recognition decision is typically on the order of tens of milliseconds. This work has obvious applications in night vision, but it is also relevant to areas such as process control, radiological, and nuclear imaging, spectroscopy, robot vision, and vehicle guidance.

1. INTRODUCTION

Often input scenes contain a vast amount of information, which tends to make pattern-recognition decisions laborious and time consuming. In traditional digital pattern recognition methods, one digitizes the input scene using a two-dimensional detector, e.g. a solid-state photodiode array, and a frame store. If the detector consists of, say, a 1000 x 1000 array of detection elements, then one has to process a million points of data. This is too much information for even very large computers to process in real time, so one generally transforms the input information into some sort of feature-space representation, e.g. through the use of edge-enhanced images, and makes the recognition decision based on this reduced data set.

An alternative approach to the pattern recognition problem is to process low-light-level (photon-limited) input images using photon-correlation methods. In this scheme photoevents are detected at the maximum rate the detection/computer system can handle. One collects photoevents until there is enough information about the input scene to achieve an acceptable error rate for the given recognition task. Our studies indicate that in many cases only a sparse sampling (a small number of detected photoevents) of the input image is needed for accurate image recognition; hence, the time needed to detect, process, and make a recognition decision can be quite short, typically a few tens of milliseconds. In effect one is letting nature randomly sample (digitize) the input scene.

The problem that a practical pattern-recognition system faces is that it must be highly sensitive to image features that will separate a given reference object from the other possible inputs, yet at the same time be insensitive to image distortions that are not important for the recognition task. It is convenient to group image distortions into two categories: geometrical and intrinsic. Geometrical distortions include variations such as rotation, scale, position, and aspect of an input image. As an example, one might want to recognize a given set of images in which the angular orientation and/or scale size can vary over a range of values. Intrinsic variations are fundamental deviations, not attributable to simple changes in geometry. In this case, the pattern-recognition task is to identify the input image as a member of an image class, rather than a specific reference image.

In this paper, we review the research to date on photon-correlation systems in which an input photon-limited image is correlated with a fixed (or deterministic) reference function stored in computer memory. The principal application for these correlation systems is automatic pattern recognition. Basically, one is given a set of possible reference images and the goal is to decide automatically (without human intervention) which of the reference objects is most like to input object. In Section 2, we briefly review the statistical properties of photon-limited imaging and photon correlation. Section 3 contains a brief description of two-dimensional, photon-counting detectors. In Section 4 and 5, correlation results obtained using an image of the reference function (matched filter case), circular-harmonic filters (rotation invariance), Fourier-Mellin descriptors (scale and rotation invariance), and maximum-likelihood filters (image classification) are summarized.

2. PHOTON STATISTICS AND PHOTON CORRELATION

2.1. Inhomogeneous Poisson processes

At low levels of illumination, an input scene $V^{\dagger}(r)$ can be represented as a two-dimensional collection of Dirac-delta functions, i.e.,

$$V^{\dagger}(r) = \sum_{k=1}^{N} \delta(r - r_k) \ , \tag{1}$$

in which r_k denotes the spatial coordinates of the k-th detected photoevent and N is the total number of detected photoevents. Of course, with an actual detector the photoelectric counts are not idealized points, but rather they occupy a finite area; the effect can be included by passing $V^{\dagger}(r)$ through a linear system in which the impulse response is equal to the point spread function of the detector[1]. Although one does not want to ignore the finite spread of the detected photoevents, it does lead to helpful simplification in the notation.

In Eq. (1), the spatial coordinates r_k of the k-th detected photoevent are random variables. The number of detected photoevents, N, may or may not be a random variable depending on how the experiments is performed. For example, N is not random for the case when a fixed number of photoevents is collected. On the other hand, if photoevents are collected for a fixed time interval τ, then from the theory of photodetection[2-6] the conditional probability distribution for detecting N photoevents in the time interval $[t, t+\tau]$ from a detector of area A, given the classical image irradiance $V(r,t)$, is an inhomogeneous Poisson process given by

$$P[N|V(r,t)] = \frac{\left[\int_t^{t+\tau} dt' \int_A d^2r\, \lambda(r,t')\right]^N}{N!} e^{-\int_t^{t+\tau} dt' \int_A d^2r\, \lambda(r,t')} \tag{2}$$

in which the rate function $\lambda(r,t)$ is

$$\lambda(r,t) = \eta V(r,t)/h\nu \ , \tag{3}$$

where η denotes the quantum efficiency of the detector, h is Planck's constant, and ν denotes the mean frequency of the incident quasi-monochromatic light.

In general, $V(r,t)$ is a random process and the conditional distribution given in Eq. (2) must be ensemble averaged to obtain the observable counting distribution. For example, if $V(r,t)$ obeys negative exponential statistics, as in the case of polarized quasi-monochromatic light emitted by a thermal source, then the observable counting distribution P(N) obeys Bose-Einstein statistics when the integration time is small compared to the coherence time of the light, see e.g., Ref. 6). However, if $V(r,t)$ does not fluctuate significantly, i.e., $V(r,t) = V(r)$, as in the case of illumination provided by a well stabilized single-mode laser, then counting distribution is simply

$$P(N) = \frac{\bar{N}^N}{N!} e^{-\bar{N}} \ , \tag{4}$$

in which

$$\bar{N} = \frac{\eta\tau}{h\nu} \int_A d^2r\, V(r) \tag{5}$$

is the average number of detected photoevents. One notes that the distribution in Eq. (4) is applicable also for polarized thermal radiation when τ is much larger than the coherence time of the light[4]. In this case the fluctuations in the irradiance are smoothed out in the time integration and V(r) represents the mean value of the irradiance.

In Eq. (1) the photoevent coordinates r_k are independent random variables. The probability density function for photoevent coordinates[6] is directly proportional to the classical intensity $V(r_k)$, i.e.,

$$p[r_k|V(r_k)] = \frac{V(r_k)}{\int_A d^2r\, V(r)} \quad . \tag{6}$$

2.2 Correlation with a Deterministic Reference Function

Our approach to the pattern-recognition problem is to calculate the correlation function formed by an input photon-limited image and a reference function stored in computer memory, which describes the object of interest. Examples that illustrate the performance of this method are given in Sections 4 and 5. In this section we summarize the salient statistical properties of the correlation signal. A detailed treatment of the statistical properties of the correlation signal is given in Ref. 7.

Consider the correlation signal

$$C(r) = \int d^2r'\, V^{\dagger}(r')\, R(r'+r) \quad . \tag{7}$$

obtained by cross correlating a photon-limited input scene $V^{\dagger}(r)$, given in Eq. (1), with a deterministic reference function R(r) stored in computer memory. Using Eqs. (1) and (7) gives

$$C(r) = \sum_{k=1}^{N} R(r_k + r) \quad . \tag{8}$$

Hence, the photon-limited correlation signal C(r) is a random function since the event coordinates r_k are independent random variables with the probability density function specified in Eq. (6). The reference function R(r) may be either real or complex. In this section R(r) is taken to be a real-valued function. The results are readily extended to the case in which the reference function is complex[8]. Also as noted above, N, the number of detected photoevents, may or may not be random depending on how the input image is sampled. Here, we take the number of detected photoevents to be fixed.

To calculate C(r), one uses the spatial coordinates of a given detected photoevent as an address. The offset coordinated r defines the location of the reference-function window within the input scene. The procedure to calculate C(r) is to look up the value of the reference function stored at the address specified by $r + r_k$, and place that value into an accumulator; this operation is repeated for all N detected photoevents. The recognition decision is based on the resulting value of C(r).

In a typical pattern-recognition problem, one would generally expect that the number of detected photoevents needed to make an accurate recognition decision would be rather large, at least a few hundred to a few thousand photoevents. As N gets large, the correlation signal in Eq. (8) tends to a Gaussian process. In the limit of large N, the probability density function for C(r) is given by

$$P[C(r)] = \frac{1}{\sigma\sqrt{2\pi}}\, e^{-\frac{[C(r) - \langle C(r)\rangle]^2}{2\sigma^2}} \quad , \tag{9}$$

in which the expected value of the correlation signal $\langle C(r)\rangle$ is

$$\langle C(r) \rangle = N \int d^2r' \, p[r'|V(r')] \, R(r' + r) \, , \tag{10}$$

the variance σ^2 is

$$\sigma^2 = N \int d^2r' \, p[r'|V(r')] \, R^2(r' + r) - \frac{\langle C(r) \rangle^2}{N} \, , \tag{11}$$

and $p[r'|V(r')]$ is given in Eq. (6). Notice that $\langle C(r) \rangle$ is directly proportional to the correlation function between the high-light-level (or classical intensity) input scene and reference function R(r).

2.2.1 Probability of Detection and False Alarm. The detection problem can be formulated by using the statistical theory of hypotheses testing[9]. On the basis of the correlation signal C(r), one must choose between two hypotheses: the null hypothesis, H_0 -- the reference function R(r) *is not* present in the input scene V(r); or the positive hypothesis, H_1 -- the reference function *is* contained in V(r).

Under hypothesis H_0, the probability density function of the correlation signal is denoted by $P_0(C) = P[C(r)|V(r') = N(r')]$, where N(r') represents a noise (or false) image. Under hypothesis H_1, the probability density function of the correlation signal is denoted by $P_1(C) = P[C(r)|V(r') = R(r')]$, where R(r') is the reference image.

Operationally, the observer usually sets a threshold value C_T for the correlation signal. If $C(r) > C_T$, hypothesis H_1 is chosen. Similarly if $C(r) < C_T$, the observer chooses hypothesis H_0. However, because of the statistical nature of the signal, the observer occasionally makes an error, regardless of the value of C_T. The probability of choosing H_1 when H_0 is true is called the probability of false alarm and is given by

$$P_{fa} = \int_{C_T}^{\infty} dC \, P_0(C) \, . \tag{12}$$

The probability of choosing H_1 when H_1 is true is called the probability of detection,

$$P_d = \int_{C_T}^{\infty} dC \, P_1(C) \, . \tag{13}$$

3. TWO-DIMENSIONAL, PHOTON-COUNTING DETECTORS

Almost all the two-dimensional photon-counting detectors that have been developed use a microchannel image intensifier[10,11] in cascade with some type of anode assembly to record the position coordinates of the event. A number of anode assemblies have been used including silicon-intensified-target television cameras[12-14], self-scanned (CCD) detector arrays[15-20], crossed-wire-grid anodes[21], multi-anode arrays[22], resistive anodes[23-27], wedge-and-strip anodes[28-31], and gray-coded masks used with a band of photomultipliers[32].

A schematic of a resistive-anode-type detector is shown in Fig. 1. An incident photon ejects an electron from a photocathode. The ejected photoelectron is directed into a stack of microchannel plates (typically arranged in a V- and/or Z-stack to prevent ion feedback) to achieve an electron gain G of approximately 10^6 to 10^8. The resulting charge pulse is collected by the resistive-anode assembly. The resistive layer is terminated by electrodes at three or four locations around its perimeter, when provide the signals for the centroiding algorithm. When coupled to position-computing electronics, the detection system is generally capable of operating at count rates up to approximately 100,000 counts per second with a spatial resolution of approximately 400 x 400 elements[24].

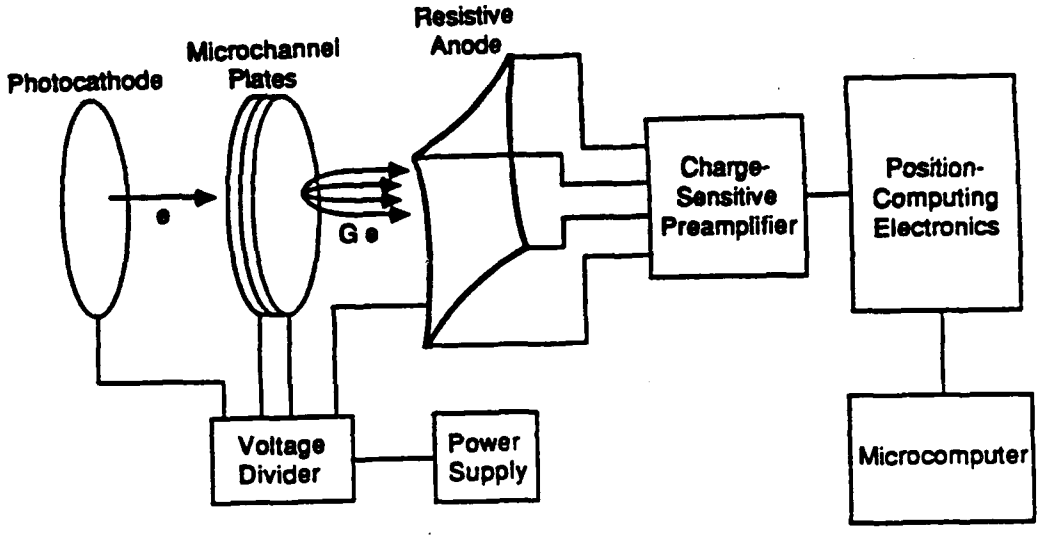

Fig. 1. Schematic diagram of a resistive-anode, photon-counting detection system.

The choice of the anode assembly, of course, depends on the requirements imposed by the application. For example, detection systems that operate with only one detected photoevent in the device at a time can be used to collect a specific number of photoevents; hence, N in Eq. (1) can be fixed, instead of random. Theses detectors can provide both the spatial coordinates and time-of-arrival information of the detected photoevents. On the other hand, detection systems that utilize a detector arrays or a television tube to read out the position coordinates of detected photoevents are generally preferable in high speed applications that involve moving objects or pulsed light sources. In these systems many events can be detected in a short time interval and then read out in a raster format, the time-of -arrival information of detected photoevents is not available, and the number of detected photoevents for a fixed time interval τ is a random variable.

4. IMAGE CORRELATION AT LOW LIGHT LEVELS

The results in Section 2 are applicable for general real-valued reference functions and input scenes[33]. The capabilities of this low-light-level approach to pattern recognition can be predicted theoretically by studying the probability density functions of the correlation signal when the input scene (1) matches the reference function stored in computer memory, and (2) is a typical background image encountered in the given application. From these probability density function, one can determine the number of detected photoevents that is required to achieve a given probability of detection and false alarm.

In this Section, we consider the correlation signal obtained when the input scene is correlated with a classical intensity image of the reference object. In the case the correlation output, C(r) in Eq. (8), corresponds to that of a matched filter. When N, the number of detected photoevents, is a fixed number, the mean value and variance of the correlation signal are given by Eqs. (10) and (11), respectively.

As an example, let us consider the recognition of detailed images, such as the engraved portraits of George Washington, Abraham Lincoln, and Andrew Jackson shown in Fig. 2. The photographs in Fig. 2 were obtained by imaging portraits from U. S. currency onto a two-dimensional, photon-counting detector [Electro-Optical Products Div., ITT Corporation, Model F4146M]. The detector was connected to position-computing electronics [Surface Science Laboratories, Model 2401] to determine the spatial coordinates of detected photoevents. The spatial coordinates of the detected events were digitized to a spatial resolution of 256 x 256 pixels and then sent to a microcomputer system for display. Illumination was provided by fluorescent room lights. Neutral density filters were inserted between the imaging lens and the detector to reduce the count rate to approximately 50,000 counts per second. In each image a fixed number of detected photoevents was collected. The number of detected events for the images in a given row are indicated along the left-hand side.

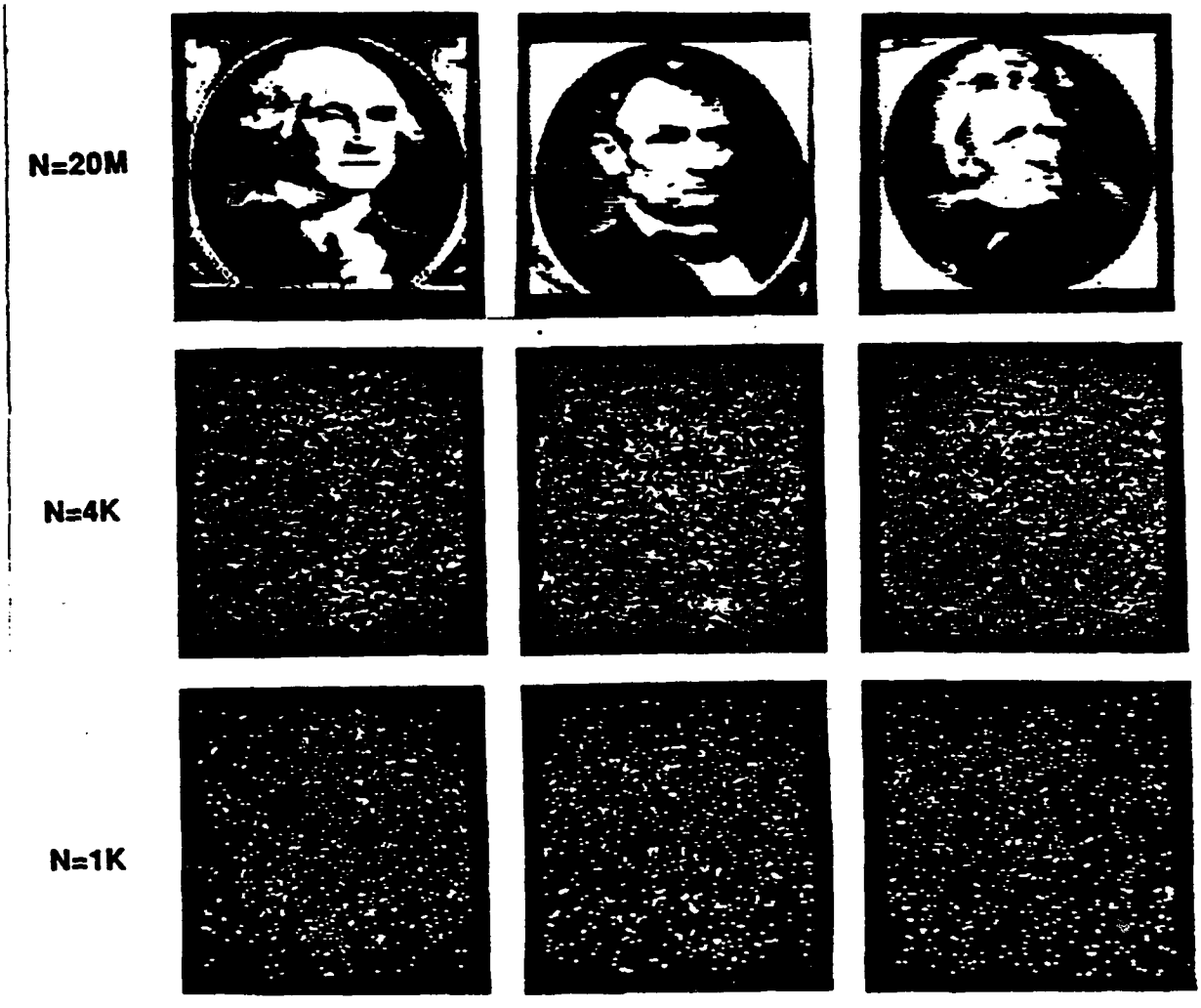

Fig. 2. Images of engraved portraits obtained using a two-dimensional, photon-counting detection system: first column, portrait of George Washington; second column, Abraham Lincoln; third column, Andrew Jackson. N is the number of detected photoevents over the entire image: top row, N = 20 million; middle row, N = 4,000; bottom row, N = 1,000. The spatial coordinates of each detected photoevent are digitized to 8-bit accuracy.

The probability density functions of the correlation signal in Eq. (8) are calculated using the images in the top row of Fig. 2. For detailed imagery one expects that the number of detected photoevents will need to be relatively large for reliable recognition; hence, the approximation that the probability density function of the correlation is Gaussian distributed should be fairly accurate.

Since the reference and input images have the same area A, we take the reference-window offset $\mathbf{r} = 0$. The mean value and variance of the Gaussian-distributed correlation signal is computed for each input object using Eqs. (10) and (11), respectively. By using the mean values and variances for the different input objects, one can calculate the probability of detection and probability of false alarm versus N, the number of detected photoevents. Figure 3 contains ROC curves for the portraits of for different values of N. The portrait of Washington was used as the reference function. From the ROC curves, one sees that excellent discrimination can be obtained by using less than one thousand detected photoevents (see bottom row of Fig. 2). It is this extreme data reduction that enables one to achieve real-time operation.

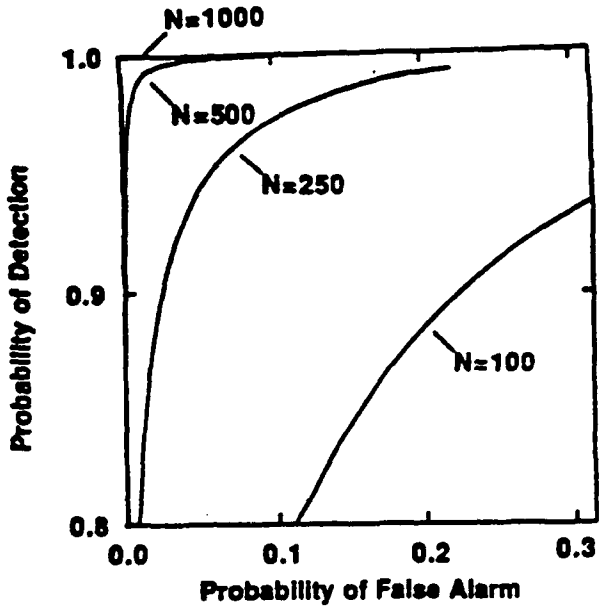

Fig. 3. ROC curves for the portraits of Washington and Lincoln for different values of N.

In operation, the recognition decision is based on a single realization of the correlation signal. N photoevents from the input image are detected, and the resulting correlation signal is compared with a threshold value C_T. If the value of the correlation signal exceeds C_T, the reference image is said to be present in the input; if not, the reference object is said to be absent. Excellent agreement between theoretical predictions and laboratory experiments have been observed. Note that at a rate of 50,000 counts/sec, the total time to detect, process, and make a recognition decision using 1000 detected photoevents is approximately 20 milliseconds.

It is important to note that in the theoretical predictions for the correlation signal, no corrections were make for additive noise or dead-time effects; these effects are simply not important when the count rate is 50,000 counts/sec and N is a a few thousand counts or less. In the experiments the dark-count rate is approximately 50 counts/sec at room temperature (a bi-alkali photocathode is used in the detector). At a rate of 50,000 counts/sec, on average, there is only one detected photoevent out of a thousand that is associated with additive noise; hence, the contribution due to additive noise is negligible.

5. DISTORTION-INVARIANT FILTERS

In most applications it is desirable to have an automatic recognition system that can tolerate certain variations in input images, which are not important as far as a recognition decision is concerned. These variations can be divided into two basic categories: geometrical distortions of the image (e.g., rotation, scale, and position) and intrinsic variations of the image (e.g. changes in illumination, image clutter and object occlusions) . One could approach this problem by using multiplexed filters in which a separate reference function (filter) is used for each scale and orientation of the input object, but this leads to a computational-intensive system design that is difficult to implement.

A more elegant approach to the problem of image distortion is to choose a reference function R(r) so that the correlation output is invariant to the distortion of the input image. Mellin transforms, which have scale- and position-invariant properties have been used[34]. Circular-harmonic filters, initially suggested by Hsu *et al.*[35], have proved useful for rotation-invariant pattern recognition [8,36-38]. Fourier-Mellin descriptors for rotation, scale and position invariance have also been reported[39-42]. Other approaches to distortion-invariant filtering include: synthetic discriminant filters[43], and the "lock and tumbler" filter[44].

Intrinsic variations within images can be treated as a problem in image classification, i.e. the input image is to be identified as a member of some category or class of images. A broader interpretation of image classification reveals that image recognition in realistic environments is always, in fact, a sorting problem. Generally, input images are subject to clutter, variations in illumination, viewing angle, defects, occlusions, etc. By treating a set of images of a given object as an image class, one can formulate the problem of image recognition in realistic environments as an image classification problem. Among the most notable statistical classification algorithms are those proposed by Fukunaga and Koontz[45], Foley and Sammon[46] and the Hotelling trace algorithm[47], all of which have been used in image-classification schemes[48-52].

In this section we consider three examples of distortion-invariant filtering at low light levels. Experimental results for circular-harmonic filters, Fourier-Mellin descriptors, and maximum-likelihood image classification are given.

5.1. Rotation-Invariance using Circular-Harmonic Filters

Any two-dimensional function $f(r,\theta)$ can be represented in terms of its circular-harmonic components as follows:

$$f(r,\theta) = \sum_{m=-\infty}^{\infty} F_m(r)\, e^{-im\theta} \quad , \tag{14}$$

where

$$F_m(r) = \frac{1}{2\pi} \int_0^{2\pi} f(r,\theta)\, e^{-im\theta}\, d\theta \quad . \tag{15}$$

In Eq. (14), $F_m(r,\theta) = F_m(r)\exp(im\theta)$ is said to be the m-th circular-harmonic component of the function $f(r,\theta)$. Rotation-invariant filtering can be achieved by taking the reference function $R(r)$, in Eq. (8), to be the complex conjugate of a single (or multiple) circular-harmonic component(s) of the reference object, e.g.,

$$R(r) = F_m^*(r,\theta) = F_m^*(r)\, e^{-im\theta} \quad . \tag{16}$$

When the offset coordinate $r = 0$, the correlation signal, $C(r,\alpha)$, is an inner product of an input function $g(r,\theta+a)$ rotated by an angle α with respect to the reference function $F_m^*(r,\theta)$:

$$C(0,\alpha) = \int_0^{2\pi} \int_0^{\infty} g(r,\theta+\alpha)\, F_m^*(r,\theta)\, r\,dr\,d\theta \quad . \tag{17}$$

Using the expansion in Eq. (14) for $g(r,\theta+\alpha)$ and substituting into Eq. (17) yields

$$C(0,\alpha) = 2\pi\, e^{im\alpha} \int_0^{\infty} G_m(r)\, F_m^*(r)\, r\,dr \quad , \tag{18}$$

in which the modulus of $C(0,\alpha)$ attains its maximum value when $G_m(r) = F_m(r)$, as given by the Schwartz inequality. Notice that only the m-th circular-harmonic component of the input contributes to $C(0,\alpha)$ in Eq. (17) owing to the orthogonality of the θ–integration, and that the rotation angle α appears only in the phase term $\exp(im\alpha)$. Hence, the modulus of $C(0,\alpha)$ is independent of the rotation angle of the input image. If the reference image is input, its orientation can be obtained from the ratio of the real and imaginary parts of the correlation signal. The rotation angle α is given by

$$\alpha = \frac{1}{m} \tan^{-1}\left[\frac{\mathrm{Im}\{C(0,\alpha)\}}{\mathrm{Re}\{C(0,\alpha)\}}\right] \quad . \tag{19}$$

which can be calculated easily when the correlation is implemented digitally. The rotation angle α is far more difficult to obtain in an optical implementation because most detection schemes are intensity based.

The magnitude of the correlation peak will depend on the particular harmonic that is chosen as the reference function. The magnitude of $C(r,\alpha)$ also depends on the location of the point about which the reference object is expanded; this location is referred to as the expansion center. The magnitude of $C(r,\alpha)$ will be an absolute maximum only when the "proper center" is chosen as the expansion center [35]. Several investigations using the centroid of the image (rather than the proper center) as an expansion center have been demonstrated to be effective for rotation-invariant image recognition[8,36,37].

Experiments to test the recognition capabilities of the photon-limited correlation scheme when a complex circular-harmonic filter is used as the reference function R(r) were performed. In the experiments 35-mm-format input scenes, illuminated by an incoherent light source, were imaged onto an ITT Model F4146M photon-counting detector. Neutral density filters were inserted to obtain a count rate of approximately 30,000 counts/sec. The (x,y)-spatial coordinates of the detected photoevents were digitized to 8-bit accuracy and sent to a digital computer for processing. The number of detected photoevents, N, (see Eq. (8)) was fixed.

Figure 4 shows the input images, the reference function, and results from the correlation experiments. The second (m=2) circular-harmonic of the vise grips, computed about the centroid of the object, is taken as the reference function. The pliers and the movable-jaw wrench are used as false objects.

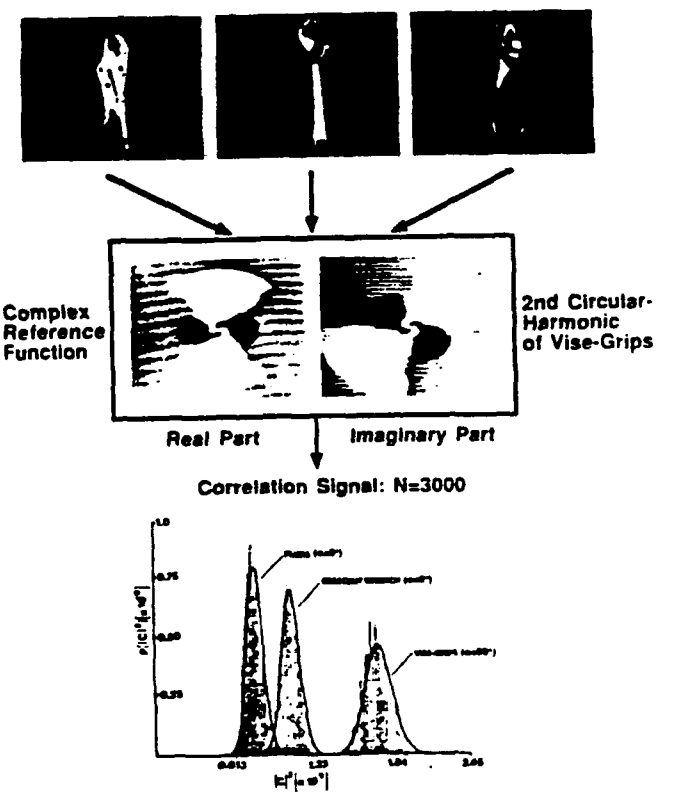

Fig. 4. Rotation-invariant filtering using a circular-harmonic filter. (a) Images used in correlation experiments, (b) the second-circular harmonic of the vise grips is used as the reference function; (c) correlation results obtained using 3000 detected photoevents.

To test the performance of the circular-harmonic filter at low light levels, correlations between photon-limited tool images and the complex circular-harmonic reference function stored in computer memory were computed. Measurements wer taken with the input reference object at various orientations (0, 90, 180 and 270 degrees with respect to the reference); the fal objects were imaged onto the detector at the orientations shown in Fig. 4. Histograms of the correlation values obtained usi 3000 detected photoevents are shown in Fig. 4. The solid curves are the theoretical predictions[8] of the probability density function for the squared modulus of the correlation signal. $|C|^2 = |C(0,\alpha)|^2$. For each input object, one thousand realizations of the correlation signal were used to calculate the histogram. In accord with theory, the magnitude of the correlation signal was found to be independent of the object-rotation angle α.

In Fig. 5, ROC curves are plotted for the vise grips (reference object) and the movable-jaw wrench (false object). Note that with N = 3000 detected photoevents, the probability of error is extremely small (approximately one error in 100,000 realizations). Based on theoretical predictions, one finds that if the *image of the vise grips* were used as the reference functio (i.e., the matched-filter case), the same discrimination capability can be achieved with approximately 1000 detected photoevents. Hence, by increasing the number of detected events by only a factor of three, one can add rotational invariance into the recognition system.

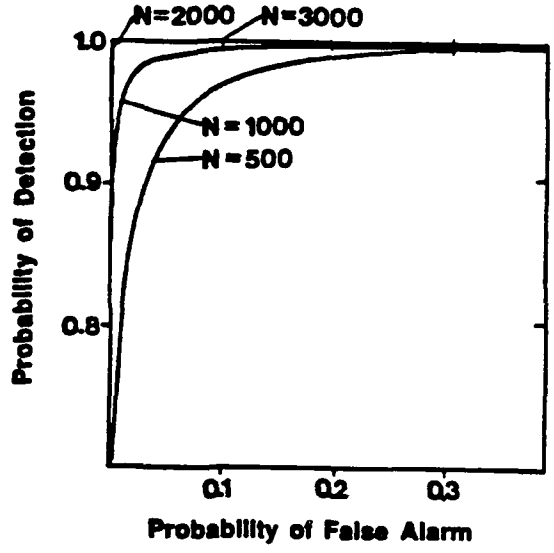

Fig. 5. ROC curves for the vise grips (reference object) and the movable-jaw wrench for different values of N.

5.2. Fourier-Mellin Descriptors

Rotation-, scale- and position-invariant image recognition can be accomplished through the use of Fourier-Mellin descriptors (FMD's). In this method either the radial moments or the radial Mellin transform of dominant terms in the circular harmonic expansion of a reference object are computed about the centroid of the image. The modulus of these descriptors is used to define invariant features. The invariant features of an input scene are compared with the corresponding features of the reference object. A recognition decision is based on the sum of the squared differences of the features, D^2. If D^2 is less than some pre-determined threshold value, the input is said to be the same as the reference. If D^2 exceeds the threshold, then the input is said to be different than the reference.

The invariant features $\phi_{s,m}$ of the input image $V(r) = V(r,\theta)$ are given by

$$\phi_{s,m} = \frac{|M_{s,m}|}{|M_{s,0}|} , \qquad (20)$$

where the Fourier-Mellin descriptors $M_{s,m}$ are

$$M_{s,m} = \int_0^{2\pi}\int_0^{\infty} V(r,\theta)\, r^{s-1}\, e^{-im\theta}\, dr d\theta \ . \qquad (21)$$

The modulus of $M_{s,m}$ is invariant with respect to rotation and changes in position of the input image. If the Mellin transform variable s is pure imaginary, the modulus of $M_{s,m}$ is also scale invariant. On the other hand, if the transform variable s is real (e.g. an integer), the normalization by the 0-th order descriptor [Eq. (20)] provides scale invariance.

Invariant features can be estimated using quantum-limited images in the following manner. If one chooses the reference function, which is stored in computer memory, to be

$$R(r,\theta) = r^{s-2}\, e^{-im\theta} \ , \qquad (22)$$

where the coordinates (r,θ) are taken with respect to the centroid of the input image, the mean value of the subsequent photon-limited correlation signal is given by

$$\langle C_{s,m}\rangle = \frac{N \int_0^{2\pi}\int_0^{\infty} V(r,\theta)\, r^{s-1}\, e^{-im\theta}\, dr d\theta}{\int_0^{2\pi}\int_0^{\infty} V(r,\theta)\, r dr d\theta} \ , \qquad (23)$$

where N is the number of detected photoevents. Notice that $\langle C_{s,m}\rangle$ is directly proportional to the classical intensity descriptor $M_{s,m}$ in Eq. (21). Also,

$$\frac{|\langle C_{s,m}\rangle|}{|\langle C_{0,m}\rangle|} = \frac{|M_{s,m}|}{|M_{s,0}|} = \phi_{s,m} \ , \qquad (24)$$

if different photoevents are used to compute $\langle C(s)\rangle$ and $\langle C(0)\rangle$.

The recognition capabilities of the photon-limited estimates of the FMD's were tested in laboratory experiments. A set of transparencies (35-mm format) were made using engraved portraits from U. S. currency, at relative magnifications of 1.0, 1.25, 1.5 and 1.75. These transparencies (input at various orientations) were imaged onto the two-dimensional, photon-counting detector. Five thousand detected photoevents were used to determine the location of the centroid of the input object in each case. The invariant features were computed using the reference function in Eq. (57) with s=2. The distance in feature space was computed between the quantum-limited input image and the reference image (George Washington with a relative magnification of unity). To test the theoretical predictions, one thousand measurements of the feature-space distance D^2,

$$D^2 = \sum_m [\phi_{2,m}^{input} - \phi_{2,m}^{ref.}]^2 \ , \qquad (25)$$

were performed for each input image to provide accurate estimates for the mean values and standard deviations of D^2.

It was found that radial moments of three circular harmonics (m = 1, 2, and 6) were sufficient to provide an error rate of 1 x 10^{-5} when 5000 detected photoevents were used to construct the estimates of the FMD for each value of m[42]. The probability density functions for D^2, based on experimental values for the mean values and variances of D^2 for the different input images, are shown in Fig. 6. In Fig. 6, a threshold value $D_T^2 = 0.08$ provides the error rate of 1×10^{-5} stated above.

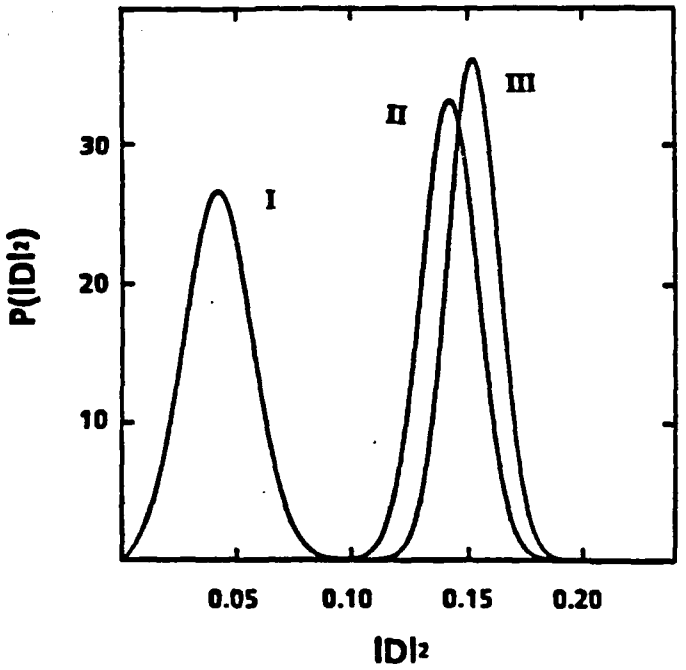

Fig. 6. Probability density functions for D^2, based on experimental measurements of the mean value and variance of D^2 for the images of Washington, Lincoln , and Jackson. The invariant features $\phi_{2,m}$ (m = 1, 2, and 6) of Washington were used as the reference.

5.3. Image Classification

In certain applications it may be desirable to ascertain the category or class of images to which an input image belongs. An image class may, for example, include images of a single scene in which variations in background content, illumination angle, and other attributes are included. Printed characters in various fonts may likewise compose a class of images. In this section photon-limited image correlation is applied to the problem of sorting two image classes. The high rate at which images can be identified arises from the efficiency of the photon-correlation calculation.

The photon-limited image consists of a histogram of the spatial coordinates of detected photoevents. Hence, a digitized photon-limited image takes the form of a two-dimensional array n. At zero offset, the cross correlation between of a photon-limited input image n and a reference function R(r) is given by

$$C = \sum_i n_i R(r_i) \quad , \tag{26}$$

where r_i represents the coordinates of the i-th pixel of the reference image and n_i is the number of detected photoevents in that pixel. In practice, most of the n_i's are zero; hence, the calculation consists simply of a summation of the values of the reference function R(r) sampled at the spatial coordinates of the detected photoevents.

Our goal is to construct a reference function R(r) that, when applied according to Eq. (26), yields useful information for class discrimination. The maximum-likelihood approach is found to be particularly well suited to the problem of sorting two classes of photon-limited images[51].

The maximum-likelihood decision criterion[52] is to choose the hypothesis corresponding to the state that was most likely to have given rise to the observed data. The central quantity in the theory is the likelihood ratio l, given by

$$l(\mathbf{n}) = \frac{p\{\mathbf{n}|H^{(1)}\}}{p\{\mathbf{n}|H^{(2)}\}} \quad , \tag{27}$$

where $\mathbf{n}$ represents the photon-limited input image and hypothesis $H^{(j)}$ (j=1,2) indicates that the input image is a member of class j. The procedure that we will use to classify an input image is as follows. When a photon-limited image $\mathbf{n}$ is input, the ratio $l(\mathbf{n})$ is calculated. To select the most probable source of the detected photoevents, class 1 is chosen when $l(\mathbf{n}) > 1$ and class 2 is chosen when $l(\mathbf{n}) < 1$.

Frequently, for convenience, the log-likelihood ratio $\ln\{l(\mathbf{n})\}$ replaces the likelihood ratio $l(\mathbf{n})$ as the decision parameter. Wernick and Morris[51] have shown that $\ln\{l(\mathbf{n})\}$ is given approximately by

$$\ln\{l(\mathbf{n})\} \cong \sum_i n_i \ln\left(\frac{[m_1]_i}{[m_2]_i}\right) + \sum_i \{[m_2]_i - [m_1]_i\} \quad . \tag{28}$$

where

$$[m_j]_i = \frac{1}{M_j} \sum_{k=1}^{M_j} s_{i,k}^{(j)} \quad . \tag{29}$$

$s_{i,k}^{(j)}$ denotes the irradiance of the i-th pixel of the k-th training image in class j, M_j is the number of training images in class j, and $[m_j]_i$ is the irradiance in the i-th pixel of the average image from class j.

Comparing Eqs. (26) and (28), it is seen that the natural logarithm term serves as the reference function for maximum-likelihood image classification at low light levels. The term involving the difference of class means is a bias, which is independent of the input image; it simply changes the threshold value of $\ln\{l(\mathbf{n})\}$ that is used to decide between the two classes. Therefore, in operation, evaluation of the log-likelihood ratio reduces to the table-lookup-and-addition procedure that we seek.

Experiments to compare the performance of various image-classification methods at low light levels have been performed[51] using images of characters and tools. Representative members of the training sets used in the character-recognition experiments are shown in Fig. 7. Reference functions were constructed for maximum-likelihood classification, the Fukunaga-Koontz transform, and average filtering. The reference function for maximum-likelihood image classification is shown in Fig. 8.

To evaluate the performance of the various algorithms we use as a figure of merit N -- the number of detected photoevents required to reduce the probability of error (i.e., the fraction of decisions that are incorrect) to 10^{-4}. The results obtained for the various classification methods are as follows: maximum likelihood, N = 146; difference of means, N = 246; Fukunaga-Koontz, N = 965. Note that the maximum-likelihood solution, Eq. (28), yields the best results.

The classification techniques illustrated above are designed for sorting of two image classes. The generalization to multiple classes is most readily obtained through application of a pairwise-voting logic, in which pairs of image classes are successively compared. On each pairwise decision, one class is eliminated. Thus, if K classes are to considered, then (K-1) correlations must be performed. In a hard-wired system, many reference function may be applied in parallel to the incoming photoevent data. The resulting correlation values may be passed to a system that implements the voting logic.

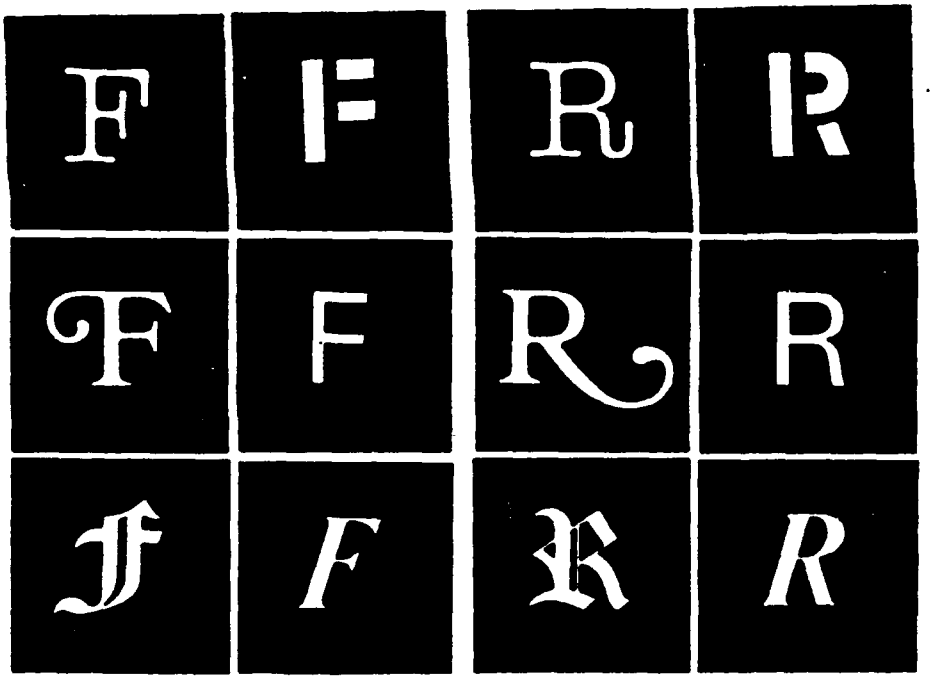

Fig. 7. Examples of images used in the experiments on image classification. In all, seven fonts were used for training and five fonts were reserved as test objects.

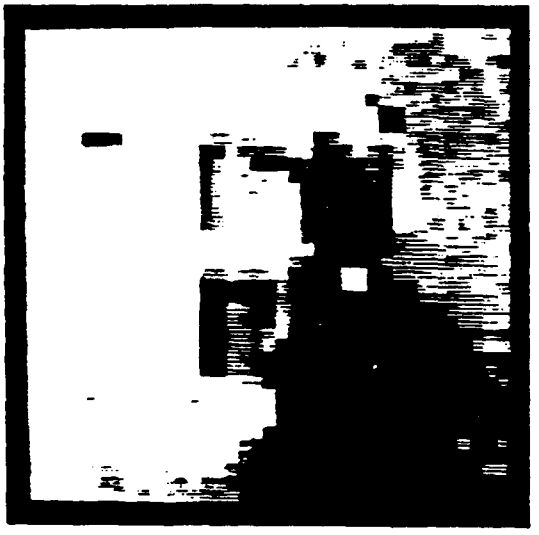

Fig. 8. Reference function for maximum-likelihood classification of F's and R's. The function contains both positive and negative values; a bias has been added for display purposes.

6. SUMMARY

At low light levels, the mean value of the photon-limited correlation signal given in Eq. (8) is directly proportional to the classical-intensity correlation function (see Eq. (10)). Hence, it is clear that if a reference filter is to work well at low light levels it must also be a good filter at classical intensities. The rational for the use of photon-limited images is two fold: (1) the input scene may be naturally photon-limited, (2) given a classical-intensity input image, because of computational efficiency in many cases it may be better to reduce the light level and use photon-correlation methods to process the images. Often only a sparse sampling (a small number of detected photoevents) of the input image is needed for accurate image recognition. The required processing (see Eq. (8)) is simply a table-lookup-and-addition procedure. Hence, if the number of detected photoevents is not too large, the time needed to detect, process, and make a recognition decision can be quite short. For example, if 1000 photoevents are needed to distinguish between a set of objects and the detection and processing system can operate at a rate of one detected photoevent every 10 microseconds, the total time needed to make a recognition decision is only 10 milliseconds.

The statistical properties of the correlation signal are summarized in Section 2. The system to compute the correlation signal C(r), formed by a photon-limited input scene and a deterministic reference function, is simply an optical implementation of a Monte Carlo scheme to calculate definite integrals.

Several reference functions for pattern recognition are examined. Examples of scene matching when the input image is correlated with an image of the reference object are given in Section 4 (see Figs. 2 and 3). In Section 5, distortion-invariant filters are considered. Experimental results that illustrate the use of circular-harmonic filters for rotation invariance (Figs. 4 and 5), rotation, scale and position invariance (Fig. 6) and image classification (Figs. 7, 8 and Table 1) are given.

The hardware requirements to implement this photon-correlation scheme are minimal. The detection system (see Section 3) consists of a two-dimensional, photon-counting detector and position-computing electronics, which is connected to a microcomputer. The reference function is stored in computer memory. Since the photon-correlation system is intensity-based, it can operate with either spatially coherent or noncoherent radiation.

There are a number of potential applications for the methods discussed in this paper. These include: machine and robot vision, target recognition from video monitors, correlation tracking for vehicle guidance, active or passive night vision, automatic recognition of spectral signatures, radiological imaging, and range extension for laser radars.

7. ACKNOWLEDGEMENTS

This work was supported in part by the U. S. Army Research Office and the New York State Center for Advanced Optical Technology.

8. REFERENCES

1. H. H. Barrett and W. Swindell, Radiological Imaging, Vol. II, Chap. 10, Academic, New York (1981).
2. L. Mandel, "Fluctuations of Light Beams," in Progress in Optics, Vol. 2, E. Wolf, ed., p. 181, North-Holland, Amsterdam (1963).
3. L. Mandel, E. C. G. Sudarshan, and E. Wolf, "Theory of Photoelectric Detection of Light Fluctuations," Proc. Phys. Soc. 84, 435-444 (1964).
4. M. Bertolotti, "Photon Statistics," in Photon Correlation and Light Beating Spectroscopy, H. Z. Cummins and E. R. Pike, eds., p. 41, Plenum, New York (1974).
5. B. Saleh, Photoelectron Statistics, Springer-Verlag, Berlin (1978).
6. J. W. Goodman, Statistical Optics, Wiley, New York (1985).
7. G. M. Morris, "Pattern Recognition using Photon-Limited Images," in Optical Computing and Processing, H. H. Arsenault and T. Szoplik, eds., Academic, New York (1988).
8. T. A. Isberg and G. M. Morris, "Rotation-invariant image recognition at low light levels," J. Opt. Soc. Am. A 3, 954-963 (1986).
9. C. W. Helstrom, Statistical Theory of Signal Detection, Chap. 3, Pergamon, Oxford (1968).
10. M. Lampton, "The microchannel image intensifier," Sci. Am. 245, 62-71 (1981).
11. O.H.W. Siegmund, K. Coburn, and R.F. Malina, " Investigation of large format microchannel plate z configurations," IEEE Trans. Nucl. Sci. NS-32, 443 - 447 (1985).

12. A. Boksenberg, "Performance of the UCL image photon counting system," in ESO/CERN Conference of Auxiliary Instruments for Large Telescopes, pp. 295-316, European Southern Observatory, Geneva (1972).
13. P. B. Boyce, "Low light detectors for astronomy," Science 198, 145-148 (1977).
14. A. Blazit, D. Bonneau, L. Koechlin, and A. Labeyrie, "The Digital Speckle Interferometer: Preliminary Results on 59 Stars and 3C 273," Astrophys. J. 214, L79-L84 (1977).
15. E. D. Loh, "A search for a halo around NGC3877 with a charge coupled detector," Ph. D. dissertation, Princeton University, Princeton, New Jersey (1977).
16. ITT Electro-Optical Products, Div. Application Note #E22, Fort Wayne, Indiana (1980).
17. C. B. Johnson and R. E. Blank, "Image tube intensified linear and area self-scanned array detectors for astronomy," Proc SPIE 290, 102-108 (1981).
18. A. R. Jorden, P. D. Read, and I. G. van Breda, "Photon counting Reticon system -- description and performance," Proc. SPIE 331, 368-375 (1982).
19. J. A. Tyson, "Low-light-level charge-coupled device imaging in astronomy," J. Opt. Soc. Am. A 3, 2131-2138 (1986).
20. E. Roberts, T. Stapinski, and A. Rodgers, "Photon-counting array detectors for the Fuse/Lyman satellite telescopes," J. Opt. Soc. Am. A 3, 2146-2150(1986).
21. E. M. Kellogg, S. S. Murray, and D. Bardas, "The high speed photicon," IEEE Trans. Nucl. Sci. NS-26, 403-410 (1979).
22. J. G. Timothy, "Multianode microchannel array detector systems: performance characteristics," Opt. Eng. 24, 1066-1071 (1985).
23. M. Lampton and C. W. Carlson, "Low-distortion resistive anodes for two-dimensional position-sensitive MCP systems, " Rev. Sci Instrum. 50, 1093-1097 (1979).
24. C. Firmani, E. Ruiz, C. W. Carlson, M. Lampton, and F. Paresce, "High-resolution imaging with a two-dimensional resistive anode photon counter, " Rev. Sci. Instrum. 53, 570-574 (1982).
25. A. H. Greenaway, A. Lyons, I. McWhirter, D. Rees, and A. Cohran, "Miniature imaging photon detector, " Proc. SPIE 331, 365-367 (1982).
26. L. Mertz, T. D. Tarbell, and A. Title, "Low noise imaging photon counter for astronomy," Appl. Opt. 21, 628-634 (1982).
27. Y. Tsuchiya, E. Inuzuka, T. Kurono, and M. Hosoda, "Photon-Counting Image Acquisition System and Its Applications," SPSE J. Imag. Tech. 11, 215-219 (1985).
28. H. O. Anger, "Survey of radioisotope cameras," Instrum. Soc. Am. Trans. 5, 311-334 (1966).
29. C. Martin, P. Jelinsky, M. Lampton, R. F. Milina, and H. O. Anger, "Wedge and strip anodes for centroid-finding position-sensitive photon and particle detectors," *Rev. Sci. Instrum. 52, 1067-1074 (1981).*
30. H. E. Schwartz and J. S. Lapington, "Optimisation of wedge and strip anodes," IEEE Trans. Nucl. Sci. NS-32, 433-437 (1985).
31. O. H. W. Siegmund, M. Lampton, J. Bixler, S. Chakrabarti, J. Vallerga, S. Bowyer, and R. F. Malina, "Wedge and strip image readout systems for photon-counting detectors in space astronomy," J. Opt. Soc. Am. 3, 2139-2145 (1986).
32. C. Papaliolios, P. Nisenson, and S. Ebstein, "Speckle Imaging with the PAPA detector," Appl. Opt. 24, 287-292 (1985).
33. G. M. Morris, "Image correlation at low light levels: a computer simulation," Appl. Opt. 23, 3152-3159 (1984).
34. D. Casasent and D. Psaltis, "Position, rotation, and scale invariant optical correlation," Appl. Opt. 15, 1795-1799 (1976).
35. Y.-N. Hsu, H. H. Arsenault, and G. April, "Rotation-invariant digital pattern recognition using circular harmonic expansion," Appl. Opt. 21, 4012-4015 (1982).
36. Y.-N. Hsu and H. H. Arsenault, "Pattern discrimination by by multiple circular harmonic components," Appl. Opt. 23, 841-844 (1984).
37. R. Wu and H. Stark, "Rotation-invariant pattern recognition using a vector reference," Appl. Opt. 23, 838-840 (1984).
38. R. Wu and H. Stark, "Rotation-invariant pattern recognition using optimum feature extraction," Appl. Opt. 24, 179-184 (1985).
39. Y. Sheng and H. H. Arsenault, "Experiments on pattern recognition using Fourier-Mellin descriptors," J. Opt. Soc. Am. A 3, 771-776 (1986).
40. Y. Sheng and H. H. Arsenault, "Noise-image normalization using low-order radial moments of circular harmonic functions," J. Opt. Soc. Am. A 4, 1176-1184 (1987).
41. R. Wu and H. Stark, "Three dimensional object recognition from multiple views," J. Opt. Soc. Am. A 3, 954-963 (1986).

42. T. A. Isberg and G. M. Morris, "Invariant Pattern Recognition Using Quantum-Limited Images," OSA Tech. Digest 12, 77-80 (1987).
43. D. Casasent, "Unified synthetic discriminant function formulation," Appl. Opt. 23, 1620-1627 (1984).
44. G. F. Schils and D. W. Sweeney, "Rotationally-invariant correlation filtering for multiple images," J. Opt. Soc. Am. A 3, 902-909 (1986).
45. K. Fukunaga and W. L. G. Koontz, "Application of the Karhunen-Loeve expansion to feature selection and ordering," IEEE Trans. Comput. C-19, 311-318 (1970).
46. D. H. Foley and J. W. Sammon, Jr., "An optimal set of discriminant vectors," IEEE Trans. Comput. C-24, 281-289 (1975).
47. K. Fukunaga, Introduction to Statistical Pattern Recognition, p. 260, Academic, New York (1972).
48. J. R. Ledger and S. H. Lee, "Image classification by an optical implementation of the Fukanaga-Koontz transform," J. Opt. Soc. Am. 72, 556-564 (1982).
49. Z.-H. Gu and S. H. Lee, "Optical implementation of the Hotelling trace criterion for image classification," Opt. Eng. 23, 727-731 (1984).
50. D. Casasent and V. Sharma, "Feature extractors for distortion-invariant robot vision," Opt. Eng. 23, 492-498 (1984).
51. M. N. Wernick and G. M. Morris, "Image classification at low light levels," J. Opt. Soc. Am. A 3, 2179-2187 (1986).
52. J. L. Melsa and D. Cohn, Decision and Estimation Theory, McGraw-Hill, New York (1978).

CENTER FOR NIGHT VISION AND ELECTRO-OPTICS
LASER RADAR AND THE DATA SET

LASER RADAR AND THE DATA SET

NIGHT VISION

RECORDS AVERAGE DISTANCE

FIELD OF VIEWS

PASSBAND NOISE

AMBIGUITY INTERVAL

LIMITED DATA SET

- TWO ASPECTS
- THREE TARGETS

NIGHT VISION

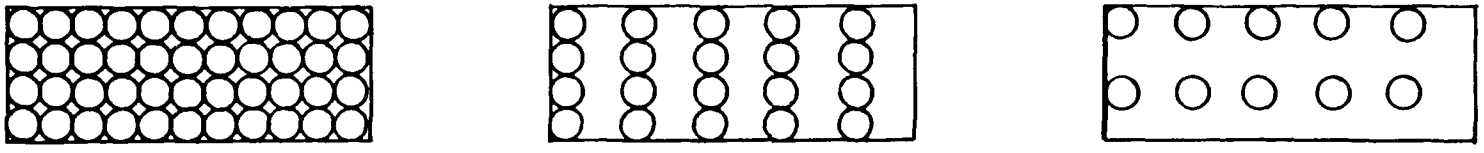

1a) 1b) 1c)

FIGURE 1 a) SHOWS SAMPLING RATE FOR RASTER SCAN OF .1 mrads × .1 mrads

b) SHOWS SAMPLING RATE FOR RASTER SCAN OF .2 mrads × .1 mrads

c) SHOWS SAMPLING RATE FOR RASTER SCAN OF .2 mrads × .2 mrads

LASER RADAR IMAGERY

RANGE INTENSITY IMAGE

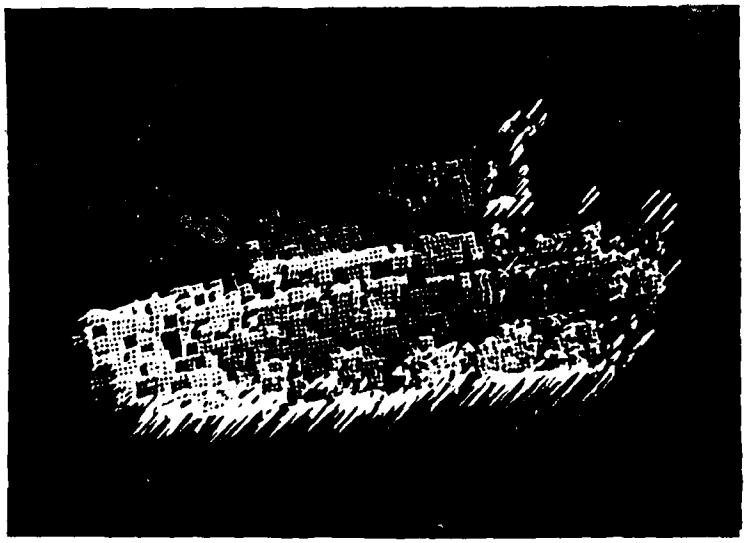

3-D SURFACE PLOT OF TANK

LASER RADAR IMAGERY

RANGE INTENSITY IMAGE

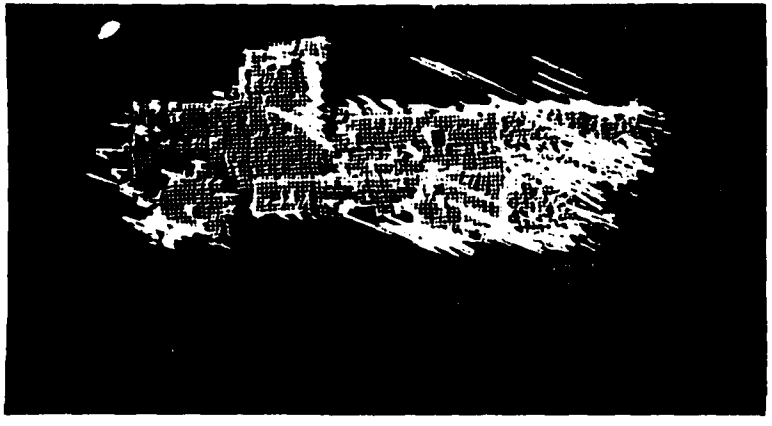

3-D SURFACE
PLOT OF TANK

MODEL BASED MULTI-SENSOR ALGORITHM DEVELOPMENT

TRADITIONAL METHODOLOGY :

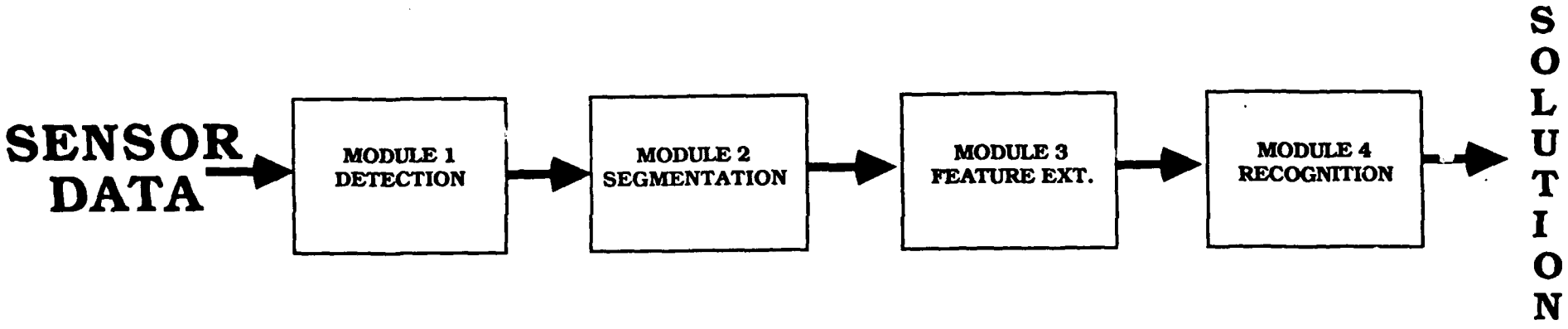

- **DECOUPLING OF INFORMATION/INFORMATION IS LOST FROM MODULE TO MODULE**
- **NOT EASILY EXTENDED TO INCLUDE OTHER SENSORS**
- **SENSOR DATA USED TO VALIDATE ALGORITHM**

MODEL BASED MULTI-SENSOR ALGORITHM DEVELOPMENT

NEW METHODOLOGY:

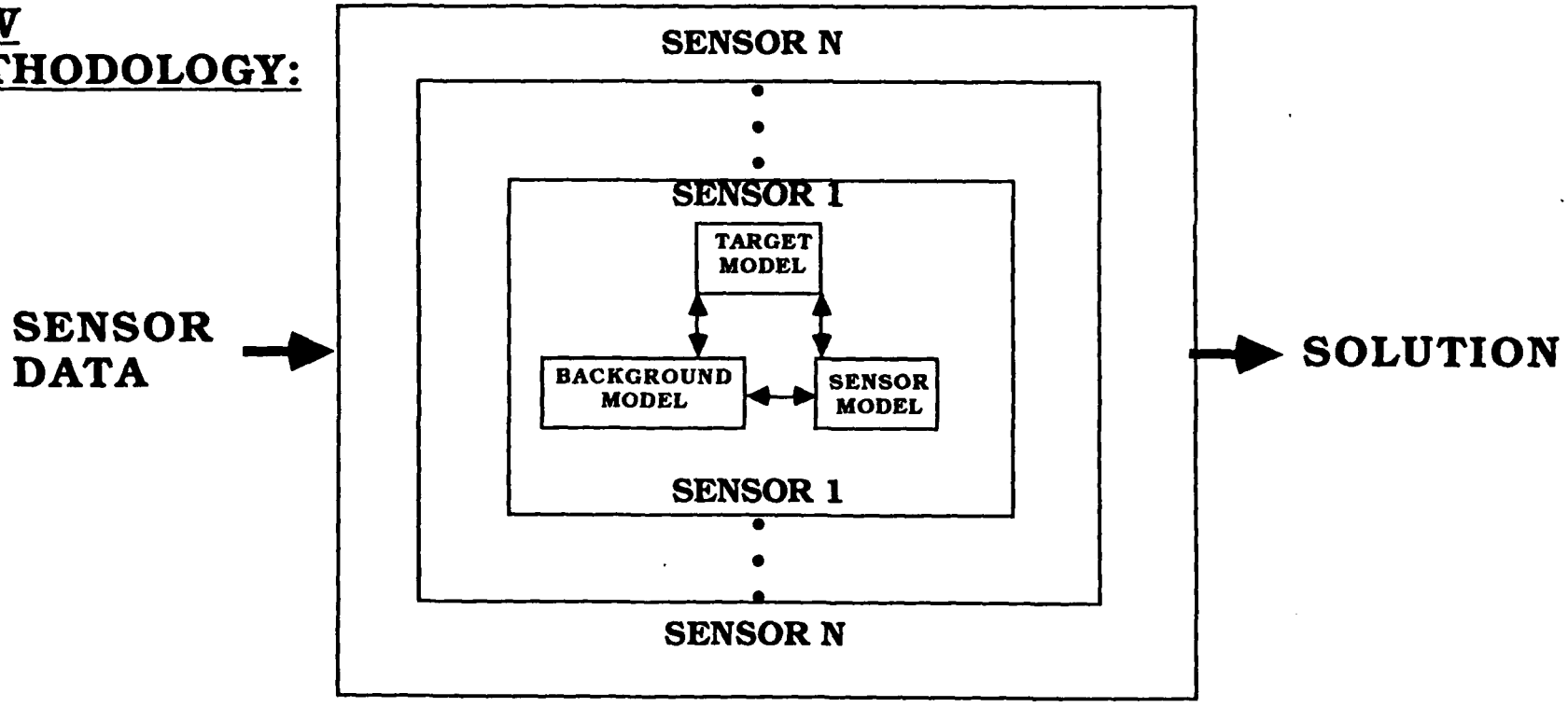

- COUPLING OF INFORMATION/NO LOSS OF INFORMATION
- EASILY EXTENDED TO INCLUDE OTHER SENSORS
- SENSOR DATA USED TO VALIDATE MODEL

LIST OF ATTENDEES

4. LIST OF ATTENDEES

OPTOELECTRONIC WORKSHOP

QUANTUM LIMITED IMAGING AND IMAGE PROCESSING

July 12, 1988

NAME	ORGANIZATION	PHONE
Ron Antos	UR, Optics	716 275-4179
L.N. Durvasula	CNVEO	703 664-1064
Nicholas George	UR, Optics	716 275-2417
Tom Isberg	UR, Optics	716 275-8385
Teresa A. Kipp	CNVEO ACD	703 664-5635
Joe Kitrosser	CNVEO ACD	703 664-5207
Martin Lahart	CNVEO ACD	703 664-5207
Mike Morris	UR, Optics	716 275-5140
Vincent Mirelli	CNVEO ACD	703 664-5635
Henry Mayfield	CNVEO	
Mark Norton	CNVEO	703 664-1968
Richard J. Peters	CNVIO	703 664-6066
Greg Salamo	CNVEO	
Geoff Sawyer	CNVIO	703 664-6066
David Singer	CNVEO ACD	703 664-6066
Tom Stone	UR, Optics	716 275-7834
Edward Watson	UR, Optics	716 275-7749
Miles Wernick	UR, Optics	716-275-8385
Tim Williams	CNVEO	703 664-6066